Appendix A

Experimental Results with Thick Barrier Buckets in the SPS

As has been shown in the preceding chapters, the application of the barrier bucket technique in a circular accelerator requires a special broadband RF installation, being capable to transfer nearly arbitrary RF amplitude to the beam. None of the CERN accelerators is however equipped with such an RF system.

The Super Proton Synchrotron (SPS) is a synchrotron to accelerate protons from some 14 GeV up to 450 GeV located at CERN. It has a circumference of 6911.5 m [230]. Originally the SPS was constructed for experiments with fixed targets. In the near future its main role will be to serve as proton and heavy ion injector for the LHC [148, 231, 232].

For beam acceleration, the SPS is equipped with a so called traveling wave RF system working at 200 MHz, the 4620th harmonic of the revolution. This system is operated as a waveguide coupled to the beam and has the advantage that its filling time is well below the revolution period. The RF amplitude can be controlled on a turn-to-turn basis which offers new possibilities for RF manipulations. In fact, thick barrier buckets can be generated by filling and depleting the traveling wave cavities several times per revolution. Thick means that these barriers have a sub-structure given by the resonance frequency at which the RF system is operated, namely 200 MHz. The potential barrier itself evolves from the amplitude modulation of the fast RF oscillation at the resonance frequency of the cavities.

This thick barrier bucket technique has already been tested successfully with low beam currents at 14 GeV (below transition) in the SPS at CERN in 1999 to check its prospects for a future upgrade [233, 234] in the framework of the CERN Neutrino to Grand Sasso project (CNGS). At that time the performance was limited by intensity effects. However, since the SPS has undergone a major impedance improvement program during the last few years [235], it was suggested to repeat the machine development experiment above the transition energy and with increased beam intensity. The chapter is based on the results of the machine development experiment as reported in [236, 237].

After an introduction to the beam dynamics of thick barrier buckets, their generation in the SPS is described. The experimental results are presented and commented afterwards. Finally, beam loading issues are discussed in the last part of this chapter.

A.1 Hamilton beam dynamics of thick barrier buckets

Pulsing the TW structures in the SPS with a constant power delivered by their power amplifiers means that the total cavity voltage rises nearly linearly with time, because the group velocity along the cavity length is constant. The normalized potential $W(\phi)$ as defined in Chapter 2 generated by the RF system can then be described by

$$W(\phi) = \begin{cases} \frac{1}{\phi_p}[\sin(\phi_q+\phi)+(\phi_p-\phi_q-\phi)\cos(\phi_q+\phi)-\sin\phi_p]\,, & -\phi_q \le \phi < -\phi_q+\phi_p \\ 0\,, & -\phi_q+\phi_p < \phi < \phi_q-\phi_p \\ \frac{1}{\phi_p}[\sin(\phi_q-\phi)+(\phi_p-\phi_q+\phi)\cos(\phi_q-\phi)-\sin\phi_p]\,, & \phi_q-\phi_p \le \phi \le \phi_q \end{cases} , \tag{A.1}$$

where the phase definitions ϕ_p and ϕ_q were chose according to Fig. A.1. Using the Hamiltonian from Eq. (2.24) with $(\phi, \dot{\phi})$ as the canonical conjugate pair of variables leads to phase space trajectories which are given by

$$\dot{\phi}(\phi) = \sqrt{2\omega_s^2[W_0 - W(\phi)]} \quad \text{with} \quad W_0 = W(\phi_l) \quad \text{or} \quad W_0 = W(\phi_u)\,, \tag{A.2}$$

where ϕ_l and ϕ_u are the limits of the trajectory in ϕ. A typical normalized longitudinal phase space is shown in Fig. A.1.

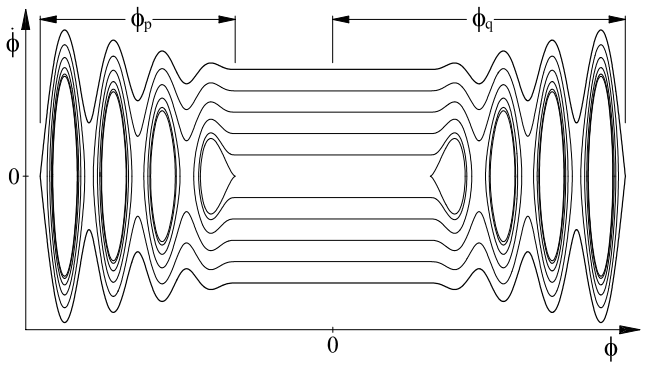

Fig. A.1: Sketch of the longitudinal phase space for a thick barrier bucket with $\phi_q = 12\pi$ and $\phi_p = 8\pi$. It can be seen that the energy acceptance is largest at the bucket ends. The inner trajectories show that separated sub-buckets exist inside the barrier.

A.1.1 Bucket height

Over most of its length the energy acceptance of a thick barrier bucket with a given RF voltage U_0 is reduced by a factor of $\sqrt{2}$ with respect to the energy acceptance of a single sinusoidal barrier bucket ($\Delta\hat{E}_{\text{harmonic}}$). This can be understood by observing that the potential created by the thick barriers is symmetric around the potential during the coasting beam section of the long bucket. Only half of the RF voltage can therefore contribute to the potential and the energy acceptance is lowered. It can be written as

$$\Delta\hat{E} \simeq \sqrt{\frac{pR\,eU_0\omega_0}{\pi h|\eta|}}\,, \tag{A.3}$$

where p is the beam momentum, R is the mean machine radius, ω_0 is the revolution frequency, $h = \omega_{\text{rf}}/\omega_0$ the harmonic number and $\eta = 1/\gamma_{\text{tr}}^2 - 1/\gamma^2 = 6.2 \cdot 10^{-4}$ is the phase slip factor. At the edges of the bucket, the energy acceptance gradually grows by the missing factor $\sqrt{2}$ to the same energy acceptance as in a harmonic RF system.

A.1.2 Bucket area

The exact bucket area of a thick barrier bucket can be calculated by numerical integration over the separatrix. For barriers which were generated in the SPS, the RF frequency is much higher than the frequency of the amplitude modulation, and it takes about 120 RF periods to fill the RF cavities. In this case a simple analytical approximation for the bucket area of a barrier bunch can be found by averaging over the bucket substructure.

The principle of such an approximation is shown in Fig. A.2. As the voltage in the cavities

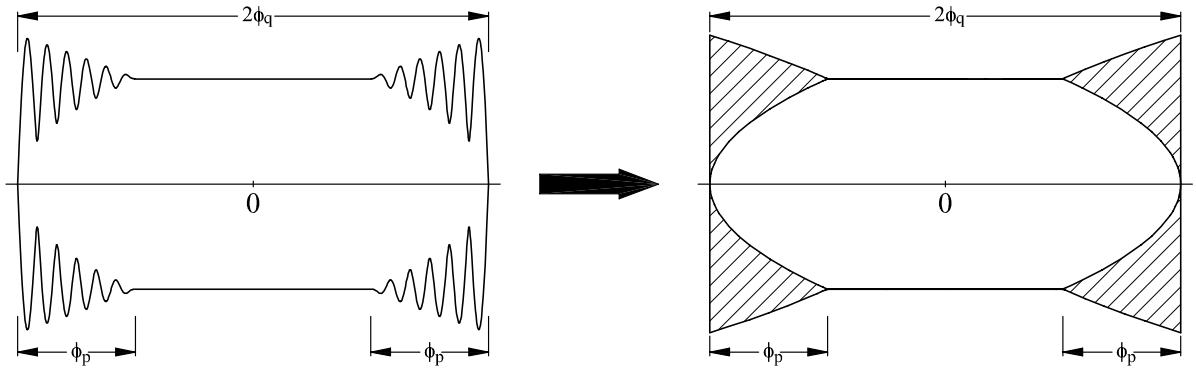

Fig. A.2: Sketch of phase space and approximated phase space for the bucket area estimation. Only half of the hatched areas are taken into account for the bucket area.

is rising linearly during filling and depletion, the minimum and maximum functions in the right picture of Fig. A.2 that define the areas of which approximately one half is inside the bucket, can be calculated analytically and are of $\sqrt{1 \pm a(\phi - b)}$ type, where a and b are parameters depending on ϕ_p and ϕ_q.

From the approximation presented in Fig. A.2 (right) the bucket area in units of $[\phi \cdot \dot{\phi}] = \mathrm{rad}^2/\mathrm{s}$ can be written as

$$\begin{aligned} A &= 4\sqrt{2}\omega_s \left[(\phi_q - \phi_p) + \frac{2}{3}\phi_p \right] + \frac{1}{2} \cdot 4\sqrt{2}\omega_s \left[\frac{4}{3}(\sqrt{2} - 1)\phi_q \right] \\ &= 4\sqrt{2}\omega_s \left[\phi_q + \left(\frac{2\sqrt{2}}{3} - 1 \right) \phi_p \right] \end{aligned} \tag{A.4}$$

and as

$$A = 4\sqrt{2}\, \frac{E\beta^2\omega_s}{h^2\omega_0^2|\eta|} \left[\phi_q + \left(\frac{2\sqrt{2}}{3} - 1 \right) \phi_p \right] \tag{A.5}$$

in conventional units of $[\mathrm{time} \cdot \mathrm{energy}] = \mathrm{eV} \cdot \mathrm{s}$.

A.2 Generation of thick barrier buckets

Unlike other circular accelerators where special broad band cavities had to be installed for barrier bucket operation, a special form of these longitudinal potential wells can be generated in the SPS thanks to the short filling time of the RF cavities with respect to the revolution period. The standard acceleration system in the SPS consists of four accelerating cavities each of which is composed of either 43 or 54 cells. As these cavities are operated in traveling wave

(TW) mode, the filling time, which is 567 ns for the two structures with 43 cells and 712 ns for the two 54 cell cavities, is much shorter than the revolution time of 23.1 μs.

By switching the amplifiers of the TW cavities on and off twice during each revolution period for some 800 ns, RF wave packages with about 1.4 μs length and a 200 MHz substructure are formed, actually a simple fast amplitude modulation of the 200 MHz RF signal. The RF voltage in the cavity is increasing and decreasing linearly as the group velocity (cf. Tab. A.3) along the TW cavities is constant. An overview of the special pulse generation electronics and the

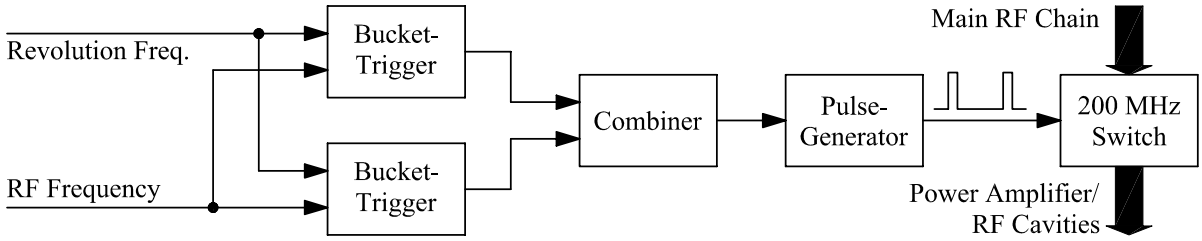

Fig. A.3: Sketch of the thick barrier bucket generation in the SPS. The 200 MHz RF signal is modulated by a switch which is triggered twice per revolution. The main RF power chain passes through the 200 MHz switch on the right of the diagram. The linearly increasing and decreasing voltage ramps in the RF structures are caused by the finite filling time.

amplitude switching of the TW cavities is given in Fig. A.3. Switching the drive voltage on and off for about one filling time generates amplitude functions which are nearly linear. It is worth noting that because of this special kind of barrier bucket generation, the phase of the 200 MHz stays constant with respect to the revolution frequency and only the amplitude of the cavity voltage is modulated. This becomes important when the phase position of the RF barrier is varied (cf. Sec. A.6).

The typical RF voltage function composed of the vector sum of all four TW cavities at zero beam current is shown in Fig. A.4. The driving pulses and the beam signal of a stationary long bunch measured with an electrostatic broadband pick-up are presented in Fig. A.5. It is clear that the RF power amplifiers cannot be switched on instantaneously and the measured voltage profile shows that the RF amplitude in the cavities does not raise perfectly linearly. Because of different cable lengths, the two traces are shifted by an arbitrary phase against each other. In fact, both barrier pulses are arranged symmetrically around the beam pulse. The distance between the two pulses, which is approximately equal to the bunch length, was set to about 3.4 μs. It was chosen to be about twice as long as the injected batch of 72 bunches (1.8 μs) from the PS. The slope on the beam pulse in Fig. A.5 arises due to the baseline drift of the broad band pick-up with its amplifier. The low frequency cut-off is at a few kHz.

A.3 Beam parameters

All barrier bucket experiments were carried out with one batch of the standard LHC beam injected in the SPS at an energy of 26 GeV. Since beam with the nominal LHC intensity was observed not to be held inside the barrier bucket, the injected intensity was decreased to about one third of the nominal number of particles. All relevant beam and machine parameters during the barrier bucket experiment are summarized in Table A.1.

The RF frequency was matched to the injected beam energy but was slightly varied during the experiment to compensate for energy mismatch. Compared to the first measurements

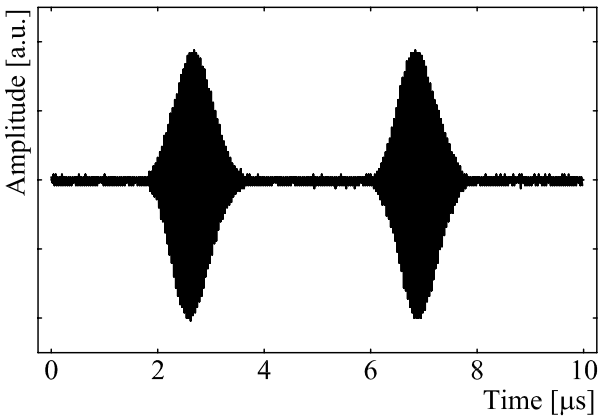

Fig. A.4: Vector sum of the cavity voltage produced by two TW cavities in barrier bucket mode. The peak voltage of the barriers is approximately 2 MV.

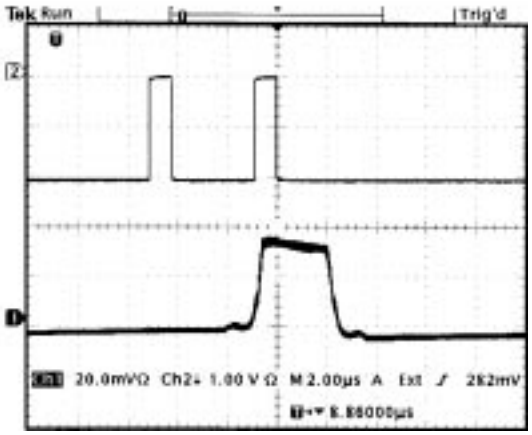

Fig. A.5: Driving pulses for the RF switch to trigger generate the barriers in Fig. A.4 (upper trace). In between the two barriers a long bunch with homogeneous line density is kept (lower trace).

Injected beam parameters:		
Momentum, p	[GeV/c]	26
Intensity per bunch (total), N		$\lesssim 0.4 \cdot 10^{11}$ ($\lesssim 2.9 \cdot 10^{12}$)
Bunch length, τ	[ns]	4
Momentum spread, $\Delta p/p$		$\pm 2 \cdot 10^{-3}$
Longitudinal bunch emittance, ε_l	[eVs]	0.35
Batch length	[μs]	1.8
	[$2\pi R_{\mathrm{SPS}}$]	1/12.8
Barrier bucket parameters:		
Harmonic number, h		4620
Frequency of RF systems, $f = h\omega_0/(2\pi)$	[MHz]	200.265
Driving pulse length of barrier excitation	[μs]	0.9
Total RF pulse length	[μs]	1.5
Total cavity voltage of two/four TW cavities, U_0	[MV]	2/4
Distance between barrier pulses	[μs]	3.3 – 4.3

Tab. A.1: Beam and machine parameters during the barrier bucket experiment. The number of injected protons corresponds to approximately one third of the nominal LHC beam intensity.

described in [233, 234], the new measurements mainly differ in the intensity per bunch ($4 \cdot 10^{10}$ instead of at the utmost $2.5 \cdot 10^{10}$ resp. $5 \cdot 10^{9}$ particles per 200 MHz bucket) and in the particle energy (26 GeV instead of 14 GeV) chosen for the experiments.

It is worthwhile noting that the earlier barrier bucket tests [233] have been performed below transition at 14 GeV, whereas the injection flat bottom for the LHC beam at 26 GeV is above the transition energy. The feedback and feed-forward loops around the cavity amplifier chains, which normally reduce the impedance of the RF systems, had to be switched off during barrier operation.

A.4 Properties of stationary barrier bunches

As a first experiment the behavior of a stationary long bunch kept by thick RF barriers over a long timescale in the SPS was studied. A single LHC beam batch was injected in between two barriers. The SPS was then set to coast mode, meaning that the magnetic field and the RF parameters remain constant for a timescale from minutes up to hours). In our case the longest coast was kept for about 100 minutes.

A.4.1 Stationary long bunch in the SPS

During the first few seconds after injection longitudinal particle density waves swashing back and forth between the two potential barriers generated by the cavities have been observed. This and its transient character are analyzed in detail in the subsequent section. About 10 s after injection, due to dilution in the longitudinal phase space, the beam becomes stable.

During the storage of the barrier bunch, the longitudinal beam profile, again measured with the electrostatic broadband pick-up and the 200 MHz component, detected by a cavity tuned to 200 MHz, have been recorded. Two such measurements are shown in Fig. A.6 and A.7.

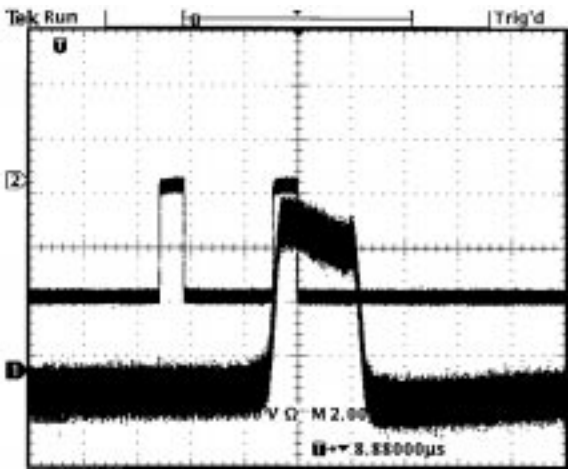

Fig. A.6: Bunch signal (lower trace) and barrier pulses (upper trace) about one minute after injection. As can be seen, the current density along the bunch is constant as expected for such a band. The slope of the line density is introduced by the low frequency limit of the broadband pick-up. The horizontal scale is 2 μs per division.

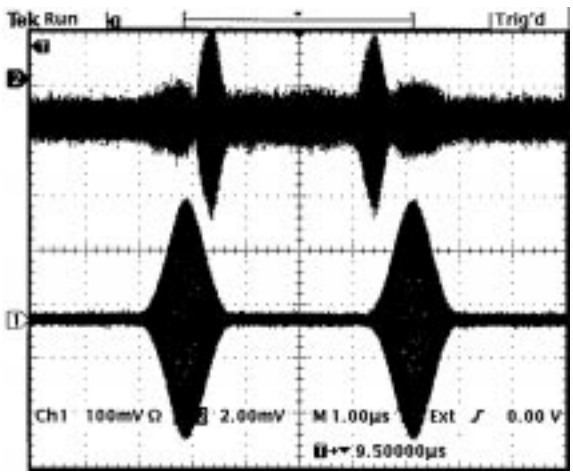

Fig. A.7: 200 MHz component of the bunch signal (upper trace) and RF voltage (lower trace) during the passage of the intentionally generated long bunch 3.5 minutes after injection. The absolute phase of the signals is not exactly the same. The horizontal scale is 1 μs per division. The beam signal should be modulated only at the bunch edges by the 200 MHz RF waveform.

The intensity at about one minute after injection was about $2 \cdot 10^{12}$ p corresponding to $2.8 \cdot 10^{10}$ p/bunch. It should be noted that the measurements by the beam current transformer include all particles circulating in the accelerator and thus the coasting beam background also contributes to the measured beam currents. The long bunch was perfectly stable at this intensity and no instability was observed during the beam storage. The beam lifetime calculated from intensity readings based on the current transformer during one of the coasts is $\tau = 1202\,\mathrm{s} \pm 80\,\mathrm{s}$.

As can be seen on the measured 200 MHz component of the beam, there are also particles outside the intentionally populated bucket. A small fraction of them are captured inside the complementary bucket situated in the rest of the circumference (see Fig. A.8) shortly after the

unmatched injection. As the line density in this bucket is also stretched around the ring, it

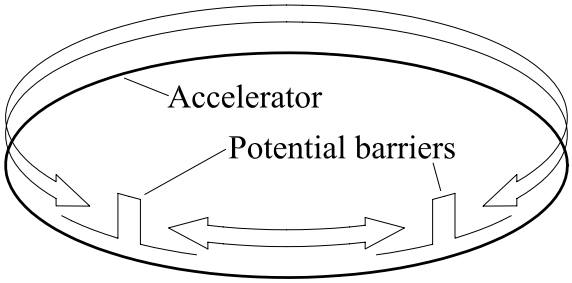

Fig. A.8: The two barrier pulses in the SPS actually generate two barrier buckets. The first bucket is intentionally built up between the two barrier pulses. The second occupies the rest of the ring.

can be estimated that the corresponding beam current is in any case below a few percent of the current in the main bucket.

A third group of particles drifts around the ring, not captured inside either of the two buckets. They were kicked onto such trajectories in the longitudinal phase plane during the first hundred turns after injection. Their large energy deviation is due to the voltage induced by the beam in the RF cavities themselves. Although situated outside buckets, their density is still modulated by the RF barriers and the particles show up as small peaks in the 200 MHz component, with maxima close to the barriers.

Theoretical parameters of barrier buckets with two and four SPS RF cavities of 1 MV each delivering bursts separated by 3.3 μs are summarized in Table A.2. In any case the bucket area

RF voltage, U_0	$\Delta\hat{E}$ ($\Delta\hat{E}_{\mathrm{harmonic}}$)	$\Delta\hat{p}/p$ ($\Delta\hat{p}_{\mathrm{harmonic}}/p$)	A_{bucket}
1 MV	53.6 (75.8) MeV	$2.14\ (3.02) \cdot 10^{-3}$	346 eVs
2 MV	75.8 (107.2) MeV	$3.02\ (4.13) \cdot 10^{-3}$	489 eVs
4 MV	107.2 (151.6) MeV	$4.13\ (5.83) \cdot 10^{-3}$	692 eVs

Tab. A.2: Barrier bucket parameters for different RF amplitudes. The total bucket length is 3.3 μs and the filling time is assumed to be approximately 600 ns. The values in brackets given for the bucket height correspond to an harmonic RF system.

is much larger than the longitudinal emittance of the injected batch which adds up to only $72 \cdot 0.35 = 25.2$ eVs. As the bunched beam debunches after the injection in the long bucket, it is obvious that the phase space density of the final bunch is at least one order of magnitude below the longitudinal particle density in nominal LHC bunches.

A.4.2 Stationary beam loading of a long bunch

The line density in a long bunch kept between two thick barriers in the SPS is much smaller than the line density of nominal LHC bunches injected from the PS. Nevertheless beam loading in the 200 MHz RF system may still influence the effective voltage delivered to the beam.

The four 200 MHz TW structures in the SPS are of backward wave type, which means that the RF power fed to the structure at its downstream end, travels in the opposite direction to the beam and is dissipated in a resistive load at the upstream end [238, 239].

The beam transfer impedance of such a structure is given by

$$Z_b = \frac{L^2 R_2}{8} \left[\left(\frac{\sin\frac{\tau}{2}}{\frac{\tau}{2}} \right)^2 - 2j\,\frac{\tau - \sin\tau}{\tau^2} \right], \tag{A.6}$$

wherein L is the interaction length and R_2 is the series impedance of the structure. The total phase slip τ is due to the velocity difference between accelerating wave and the beam:

$$\tau = \frac{L}{v_g}\left(1 - \frac{v_g}{v}\right) \cdot (\omega - \omega_r)\,. \tag{A.7}$$

The center frequency of the cavities operated in $\pi/2$ mode is defined as $\omega_r = 2\pi \cdot 200.222\,\mathrm{MHz}$, $v = \beta/c$ and v_g are beam velocity and the group velocity of the cavity structure. Some properties relevant for beam loading estimates are condensed in Table A.3. Illustrations of the beam

Center frequency of $\pi/2$ mode, $\omega_r/(2\pi)$	[MHz]	200.222
Interaction length 4/5 section cavity, L	[m]	16.082/20.196
Group velocity, v_g	[m/s]	$0.0946c$
Operating frequency at $p = 26\,\mathrm{GeV}$, $\omega/(2\pi)$	[MHz]	200.265
Beam transfer impedance 4 section cavity, Z_b	[MΩ]	$0.874 - j0.048$
Beam transfer impedance 5 section cavity, Z_b	[MΩ]	$1.38 - j0.096$
Total beam transfer impedance	[MΩ]	$4.502 - j0.288$
(two 4 section and two 5 section cavities)		$4.51\,\mathrm{M\Omega} \angle -3.67^0$

Tab. A.3: Relevant parameters of the 200 MHz TW RF system at 26 GeV/c.

transfer impedance can be found in e.g. [240]. As the frequency of operation at 26 GeV beam momentum is quite close to the center frequency, the cavity impedance is mainly resistive. The line density $\lambda(\phi)$ can be calculated according to Eq. (2.60) by assuming a distribution being parabolic in energy $f(\phi = \mathrm{const.}, \dot{\phi}) \propto (1 - \dot{\phi}^2/\dot{\phi}^2_{\mathrm{max}})^{1/2}$. It is directly proportional to the square of the energy deviation of the limiting trajectory in phase space.

The beam current along the bunch with such a distribution for an intensity of $0.35 \cdot 10^{10}$ p/bunch is shown in Fig. A.9. The voltage induced at 200 MHz by this current (averaged on a time scale of a few RF cycles) is plotted in Fig. A.10.

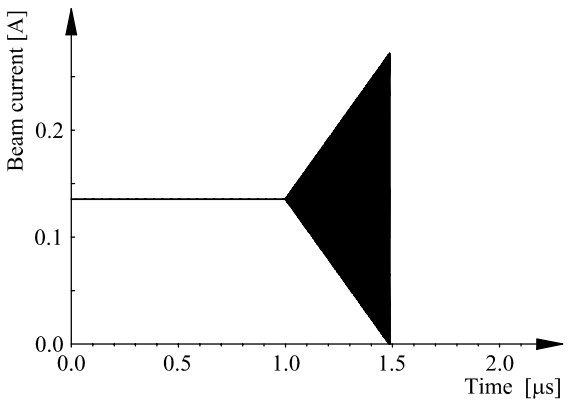

Fig. A.9: Calculated beam current versus time for a line density distribution as assumed in Eq. (2.60). The center of the bunch is at $t = 0$. In the measurements, the particle density at the edges is lower than expected because of separated islands inside the barriers which are less populated than the assumed in the model.

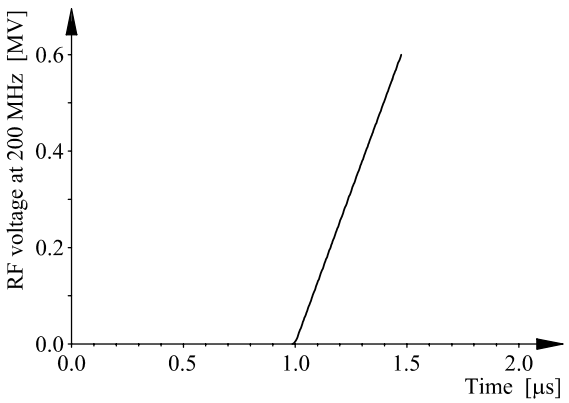

Fig. A.10: Calculated absolute beam induced voltage versus time for the distribution shown in Fig. A.9. This is only an upper estimation of the induced voltage which reduces the external cavity voltage. The measured beam induced voltage does not have the maximum at the edge of the long bunch.

If only the absolute value of the cavity impedance is been taken into account, the maximum voltage reduction induced by beam loading can be estimated to be around 0.6 MV. Compared

to the external cavity voltage of 2 MV this is not negligible. It is worth noting that part of this induced voltage is compensated by the amplitude control loop which is acting on the vector sum of all cells of one TW cavity.

The simple model mentioned above would predict a 200 MHz beam component which increases linearly along the barrier and has its maximum at the largest RF voltage. This is in fact not true because the bunch has a more complex structure of separated sub-buckets and outer trajectories (see Fig. A.1) which cover only a fraction of the whole bunch. As the outer regions of the bunch are naturally less populated, the bunch edges will be also less populated than the inner regions. Additionally, there are separated islands in phase space inside the barriers which are also less populated than assumed in the simple model. The 200 MHz beam component therefore shrinks again towards the end of the bucket.

Fig. A.7 shows that the RF component increases nearly linearly where the beam reaches the barrier and decreases again after 380 ns. The analysis of the 200 MHz beam component can give an estimation for the effective voltage seen by the beam in the RF cavities. It should be mentioned that only the DC and the 200 MHz components are the two dominant current contributions to the beam structure. All other frequency components are strongly suppressed.

The beam current distribution along the final bunch kept by the two barriers is much more homogeneous than the injected bunch structure. This causes a peak current along the coasting beam fraction of the final bunch which is about an order of magnitude lower than the peak current of the injected LHC bunches.

A.5 Transient beam behaviour after injection

As shown in the previous section, the behaviour of the long bunch held by thick barriers is as expected; a few seconds after injection equilibrium is attained. It is stable and the line density along the central part of the bunch is constant. However, the most critical process is the formation of the long bunch itself. As it is impossible to prepare a single long bunch in the PS with its present RF systems and to transfer it to a matched bucket in the SPS, an LHC-type batch is injected between the two potential wells. It consists of 72 bunches spaced by 25 ns with a bunch length of 4 ns each (see Table A.1). These bunches have a strong 200 MHz Fourier component during the first turns after injection which decays before the first particles are reflected at the barriers. As an unexpected large fraction of the injected particles was not reflected by the barriers a detailed analysis of the possible mechanism is presented below.

A.5.1 Measured profiles

To analyze the beam dynamics during the injection of a LHC batch into a long bucket, the evolution of the line density was recorded on the broadband pick-up during the first second after injection. One trace is recorded every 300 turns and the full display corresponds to the first $4.5 \cdot 10^4$ turns. Two typical measurements for 2 MV (left) and 4 MV (right) voltage are shown in Fig. A.11.

The first observation is that the injected beam spreads very asymmetrically in azimuth, most particles drifting to the left which means that their energy is below the reference energy. Moreover, only a fraction of the particles is reflected by the barriers. A non-negligible fraction of the injected beam passes through the left barrier and becomes coasting or is captured in the second, extremely long barrier bucket (assuming that the energy of some particles is above the reference energy, see Section A.4.1). Only particles with positive energy deviation can be

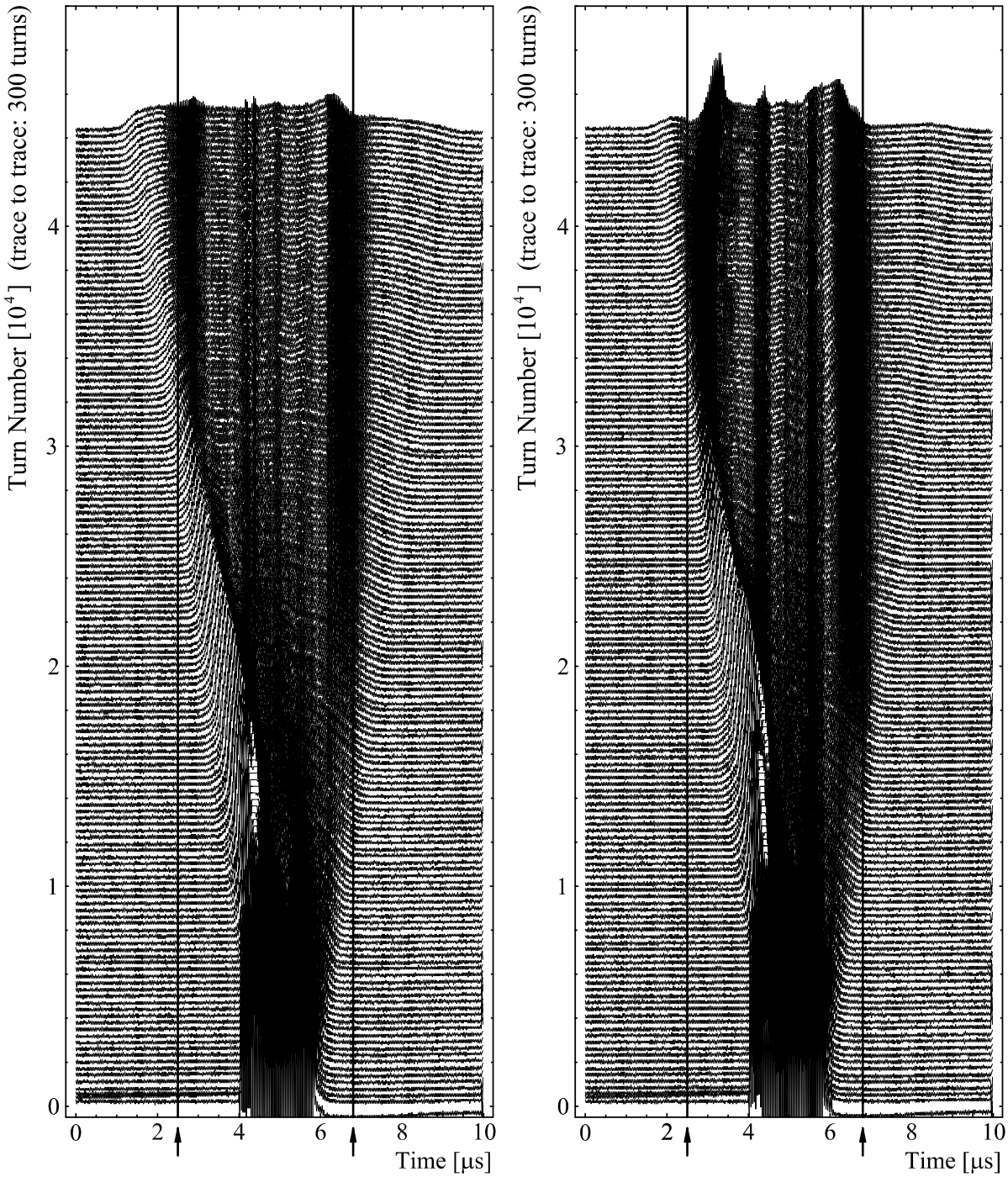

Fig. A.11: Mountain range plot of the pick-up signal during first $4.5 \cdot 10^4$ turns in the SPS. One trace was recorded every 300 turns. The left plot shows a measurement with 2 MV whereas the right plot was taken with 4 MV RF voltage. The barriers (maximum cavity voltage) are located at 2.5 and 6.8 μs (marked by thick lines). The bunches around 4.3 μs do not debunch because of a parasitic 200 MHz RF voltage burst following each barrier pulse.

captured in the second barrier bucket because they need to pass one barrier first and lose energy

so that they cannot cross a further barrier.

From the momentum spread of the injected beam given in Table A.1 and the energy acceptance in Table A.2 an RF voltage of 1 MV theoretically should have been sufficient to capture all particles of the injected beam. In this case, an effective RF voltage reduction caused by beam loading should have been compensated, but even without feedback and feed-forward loops, the total beam should have been easily captured with 2 MV RF amplitude.

The fraction of the beam crossing the left barrier is estimated by integrating over the beam profile (Fig. A.11). For an RF voltage of 2 MV, approximately 50–65 % of the injected beam has been captured in between the barrier bucket, whereas still 20 % of the particles drifting away in the 4 MV case. Furthermore, it is possible to estimate the maximum energy deviation of particles crossing the barriers by measuring the drift velocity $\dot{\phi}$ relative to the synchronous particle. In the $U_0 = 2\,\mathrm{MV}$ case, the drift velocity is about $\dot{\phi} = 4.2 \cdot 10^3\,\mathrm{rad/s}$ which corresponds to an energy deviation of 139 MeV. This deviation is indeed larger than the energy acceptance of the bucket (see Table A.2). The situation changes in the $U_0 = 4\,\mathrm{MV}$ case as particles with an energy deviation of up to $\Delta E \simeq 108\,\mathrm{MeV}$ should normally be kept inside the bucket. However, the results are intensity dependent and the precision with which the drift speed can be extracted from the measured profile is rather limited.

Energy loss by transient beam loading in the cavities is thus suspected to be the process which might explain the beam behaviour. On the one hand, particles may lose energy quickly due to the RF cavities during the debunching in the first 200 turns after injection because of transient beam loading. On the other hand, the effective amplitude in the cavities might also be lowered by an RF voltage induced by the 200 MHz component of a stationary long bunch (see Section A.4.2) in equilibrium because of transient and stationary beam loading. The first effect will be analyzed in detail in the next section.

A.5.2 Debunching process after injection

To understand the time scale on which the beam can lose energy after injection in the SPS with its uncompensated cavity impedances, it is necessary to have a closer look at the debunching procedure and especially the decay of the 200 MHz beam component.

The decay of the injected batch structure with 4 ns long bunches spaced by 25 ns caused by the dependence of the revolution period of the individual particle in the SPS is very fast. According to the equations given in Sec. 3.3.2 the debunching time at injection flat-bottom is about 1.8 ms which corresponds to 80 turns. Measurements of the beam induced voltage during the first 150 turns confirm calculations which predict that the 200 MHz beam component should decrease to below 20 % of its initial value within approximately 100 turns. The time needed for the 40 MHz and 200 MHz beam structure to decay is approximately five times longer than the debunching time t_d, because of the 25 ns bunch spacing, where every fifth bucket is populated at 200 MHz.

This decay is nevertheless much shorter than the time needed for particles from the batch to reach the barrier and thus further calculations can be assumed to be independent of any barrier RF voltages. The assumption is confirmed by the fact that, as can be seen from Fig. A.11, no further significant energy loss on a time scale of a few thousand turns is observered.

A.5.3 Estimation of the average energy loss by beam loading

The average rate of energy loss per particle can be estimated by application of energy conservation law. As mentioned before, the filling time of the 200 MHz TW structures in the SPS is

much shorter than the revolution time and the cavities have thus no memory from turn to turn. Each time the batch arrives, the cavities are completely empty. Therefore, the total energy delivered by the beam to the cavity can be derived from the measured induced voltage profiles during the beam passage.

The total vector sum measured over all four TW structures in the SPS during the first turn is plotted in Fig. A.12. The voltage profiles of the beam induced voltage in between the

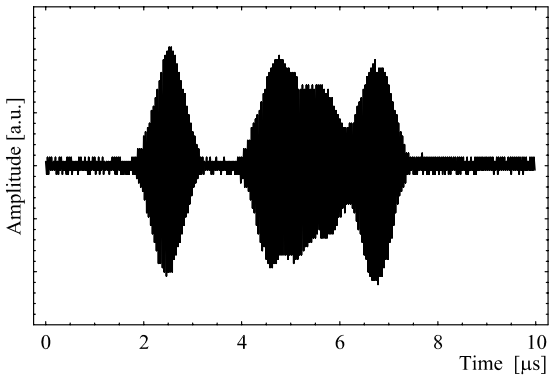

Fig. A.12: Vector sum of all four TW cavity voltages during the first passage of the LHC batch injected from the PS. It can be clearly seen that the beam induced voltage (centre) is nearly as large as the two barrier waveforms generated by the RF power amplifiers.

barriers are alike on subsequent turns, but their amplitude decreases from turn to turn [236]. Filling the TW structures with power from the beam looks similar to filling them with power amplifiers as the rate of rise of the RF voltage is the same in both cases.

To compute the average power and also the average beam energy delivered to the cavities one first has to calculate the effective voltage by integrating over the voltage function in Fig. A.12. Only the region where the cavity voltage is induced by the proton beam (between $\tau_i \simeq 4\,\mu$s and $\tau_f \simeq 6.2\,\mu$s) has to be taken into account. The effective power delivered to the cavity is then defined by

$$P_{\text{avg}} = \frac{U_{\text{eff}}^2}{|Z_b|} \simeq \frac{\dfrac{1}{\tau_f - \tau_i}\displaystyle\int_{\tau_i}^{\tau_f} U(t)^2\,dt}{|Z_b|}\,. \tag{A.8}$$

Multiplying the effective power P_{avg} by the time interval of integration $\tau_f - \tau_i$ gives the total energy which was delivered to the RF system and which was thus lost by the beam at every turn.

For conversion to more convenient units, this can be normalized per proton. The result is given in Fig. A.13. The decay of the beam induced power was fitted by a second order

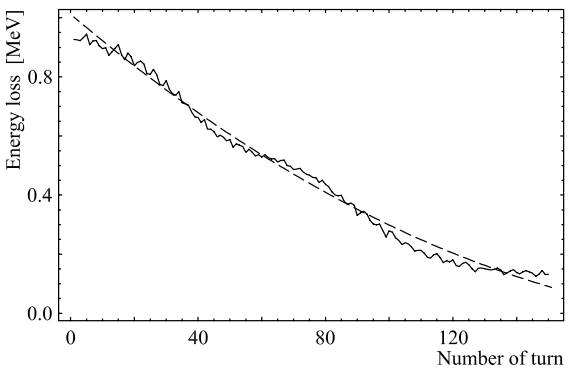

Fig. A.13: Average energy loss per proton per turn versus number of turns normalized to an intensity of $0.4 \cdot 10^{11}$ particles per bunch. The dashed line is a fit to the measured curve and is used for the total energy loss estimate.

polynomial. The energy losses after the first 200 turns are negligible.

Integration over the fitted function therefore gives a good approximation of the total energy. For one injected LHC-type batch with $0.4 \cdot 10^{11}$ protons per bunch this assumption gives

$$\Delta E_{\mathrm{avg}} \simeq 72\,\mathrm{MeV/p}\,. \tag{A.9}$$

This mean energy loss per particle is below the energy deviation of the particles crossing the potential barrier as observed in Fig. A.11 which is above 100 MeV. However, some particles receive a much larger energy kick whereas others experience no significant net energy loss. Moreover, the bunches are not only shifted by a certain amount of energy but also blown up enormously. A simulation of an LHC-type bunch with parabolic distribution in phase and energy was made to check the blow up in energy spread. One bunch of 2000 particles was placed at the crest of the RF voltage and tracked for 200 turns (Fig. A.14) while the RF amplitude was reduced. As the RF amplitude decreases linearly to zero within these 200 turns this situation

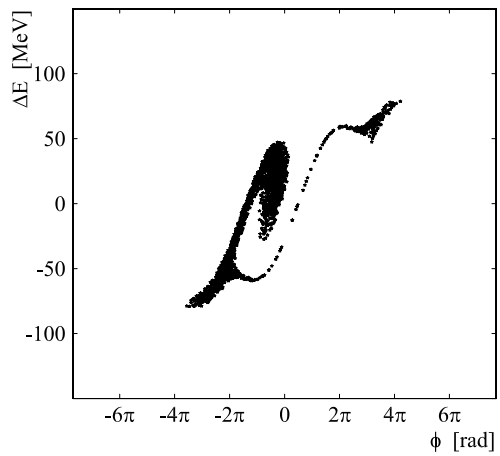

Fig. A.14: Distribution of an LHC bunch placed at the crest of the RF voltage which linearly decreases to zero within 200 turns. In this example, 2000 particles are tracked. The initial bunch distribution was parabolic in phase and energy.

should give a good estimation for the blow-up in energy spread. If a further energy shift of the center of gravity of the bunch by ΔE_{avg} is assumed which is not included in the tracking, the energy deviation of particles crossing the barriers in the range of some 140 MeV observed from the mountain range plots (Fig. A.11) becomes explicable.

Knowing the total average energy lost by the beam, it is possible to roughly estimate which fraction of the injected batch can be captured in the barrier bucket and which fraction becomes coasting. It is assumed for simplicity that the whole batch is shifted by the average energy loss ΔE_{avg}. It is clear that in reality not all bunches are shifted equally (see Fig. A.14). Some of them receive much larger kicks in energy whereas others stay close to their initial energy. Averaging over the whole batch should however lead to the correct order of magnitude. The barrier bucket in which the batch is injected simply defines a certain, allowed energy range $\pm\Delta\hat{E}$. As long as particles stay inside this energy range they are assumed to be captured.

With a total average energy loss of 72 MeV per particle and an external barrier RF voltage of 2 MV one computes with this method that 39 % of the injected particles should be captured in between the two barriers. In the case of 4 MV RF voltage about 83 % of the injected particles should have been captured. Stationary beam loading has been taken into account. Even though this should be only regarded as a rough estimation because of many assumptions, the results agree quite well with measured values (defined in Section A.5.1).

A.6 Moving the barriers inside the long bunch

As a further experiment, it was also tried to vary the thickness of the barriers to simulate a barrier which moves in phase. Considering the hardware set-up it was however predicted that batch compression by the moving barrier should not take place.

An overview sketch of the barrier bucket generation in the SPS has been given in Fig. A.3. The RF barriers are generated by switching on and off the main 200 MHz RF chain. By doing so, only the amplitude of the 200 MHz RF structure is modulated whereas the phase of the RF signal itself always stays constant in phase with respect to beam at reference energy. If the barrier size is made variable by changing the drive pulse length, only the phase of the amplitude modulation is changed, and not the 200 MHz phase (Fig. A.16). On the contrary, for a real moving barrier the 200 MHz phase should also be shifted synchronously with the amplitude modulation phase shift (Fig A.15).

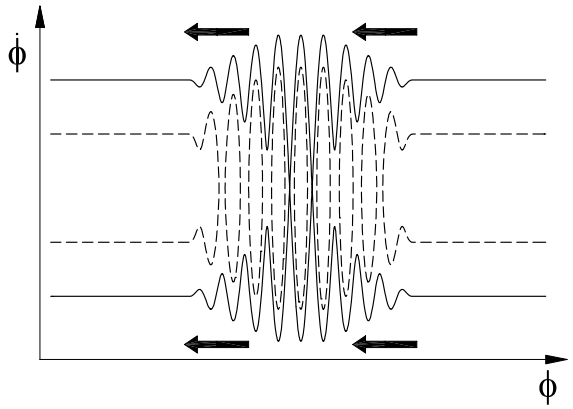

Fig. A.15: Longitudinal phase space for a moving barrier. The phase of the barrier is shifted to the left. If the phase of the amplitude modulation and also the phase at 200 MHz is shifted synchronously, the thick barrier is moved smoothly. Virtually no particles penetrate the barrier and batch compression is possible.

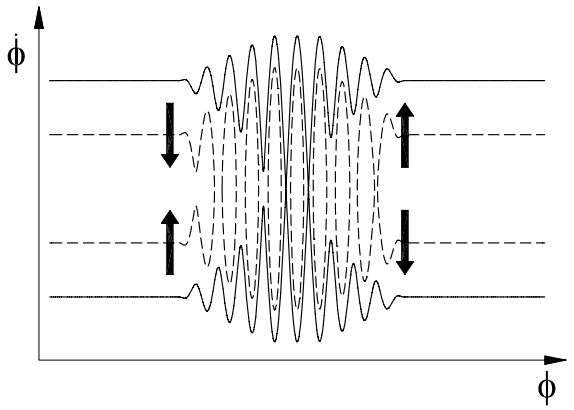

Fig. A.16: Scheme applied in the SPS: same longitudinal phase space as in Fig. A.15 but only the phase of the amplitude modulation is moved now while the 200 MHz phase stays constant. Moving the amplitude modulation to the left, some populated phase space is separated from the main bunch and penetrates into the barrier.

Changing only the phase of the RF amplitude modulation as was done in SPS is not sufficient to achieve batch compression. Increasing the length of the barrier simply leads to capture of some part of the bunch into the barriers. This is exactly what has been measured. Fig. A.17 shows a long bunch which is still unbunched for about half of its length whereas half of the bunch has penetrated inside the barriers and is simply a bunched beam in stationary 200 MHz buckets. Observations in the SPS are thus in agreement with this model.

A.7 Conclusions from the barrier bucket experiment

As the barrier bucket technique is regarded to be a promising scheme to increase the luminosity in LHC, the SPS was used as test bed to study the behaviour of long bunches kept by RF barriers. A first beam experiment on barrier buckets was carried out below transition at 14 GeV, with low beam intensities and fixed target beam. During the second experiment all tests have been performed with one standard LHC batch injected from the PS above transition at an energy of 26 GeV and an intensity of $2.9 \cdot 10^{12}$ p/batch.

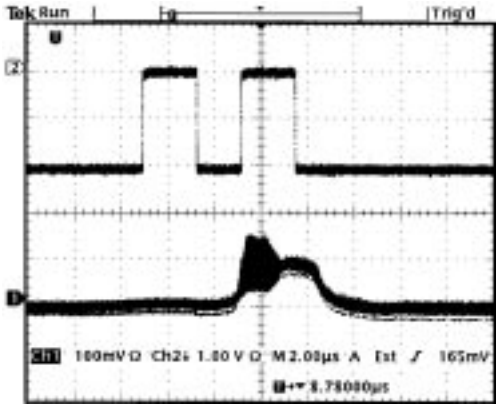

Fig. A.17: Moving only the modulation amplitude does not compress the bunch. About half of the long bunch is rather captured inside the barrier (lower trace). Initial point for this measurement was a stationary long bunch similar to Fig. A.5.

The maximum intensity, which corresponds to one third of the nominal intensity for the LHC, was limited by strong beam loading effects in the 200 MHz TW cavities. On the one hand, the large 200 MHz component of the injected batch caused transient beam loading and on the other hand, stationary beam loading reduced the effective voltage, which was available for the RF barrier. Due to the absence of feedback and feed-forward loops, the beam loading was not compensated. This can be avoided in future experiments by two possible counter measures: firstly, the transient effects during the capture process could be suppressed by capture of the LHC batch by two TW cavities with servo loops switched on, while the other two TW cavities are operated in barrier mode. After capture, the batch could be debunched adiabatically to the barrier bucket. Secondly, the injection of a debunched beam from the PS with a line density modulation as low as possible would decrease the 200 MHz component and lower the transient beam loading.

The effect of the transient beam loading during the first 200 turns after injection leads to an energy loss due to energy transferred from the beam to the 200 MHz TW cavities. Calculations for the average energy loss of the beam, which is in the range of 72 MeV per proton, are found to be in good agreement with the measured number of captured particles.

It is be shown that in the stationary case, when the transient effects had decayed a few seconds after injection, no significant longitudinal density modulation along the bunch was detected and the bunch could be kept stable for more than 80 min at the injection flat bottom. As the beam energy was widely spread by the large beam loading at injection, the particle density in the longitudinal phase space was reduced by more than one order of magnitude so that no instabilities could be observed.

The barrier bucket experiment has shown that if barrier buckets will be used in LHC, special attention has to be paid to RF gymnastics in the presence of strong beam loading. In the SPS the implementation of counter measures against the beam loading effects should allow higher particle densities to be stored in between the barriers and to observe possible instabilities in the long bunch.

Appendix B

Creation of Special Bunch Patterns in the PS Complex

The bunch combination scheme to create long and flat bunches in the LHC is based on trains of either 16 or 32 bunches with spacing of 25 ns. In between these trains, gaps of two or four non-populated bunch positions are required. Preferably, such bunch patterns should be generated directly in the PS complex so that the beam can pass the SPS without further RF manipulations. It is important to point out that the PS complex at the time of a long bunch LHC upgrade might also have undergone significant upgrades itself like the construction of a new injector linac with an energy above 2 GeV or the replacement of the PS Booster by a new rapid cycling or multi-ring synchrotron [175]. Therefore, only some basic ideas shall be given in this appendix on the means to generate the required bunch patterns required by the long bunch combination scheme.

B.1 Bunch pattern for the combination of 16 bunches

The sub-bunch pattern at the beginning of the combination can be written as $16 \otimes b \oplus 2 \otimes e$ and it fits four times into the circumference of the ring so that the full PS bunch pattern at the harmonic number $h = 84$ becomes

$$4 \otimes (16 \otimes b \oplus 2 \otimes e) \oplus 12 \otimes e\,.$$

Assuming at least one conventional bunch pair splitting on the PS flat-top this could be reduced to

$$4 \otimes (8 \otimes b \oplus 1 \otimes e) \oplus 6 \otimes e\,, \tag{B.1}$$

but afterwards no further symmetry remains. Either options can be found to intentionally remove bucket without disturbing the rest of the bunch or train or the PS must be equipped with an additional acceleration system to accelerate the protons from 1.4 GeV to 26 GeV on $h = 42$. Such an RF system must cover the frequency range from 18.4 to 20.0 MHz so that ferrite tuned coaxial resonators could be used to keep the power consumption within reasonable limits [241]. Moreover, the PSB RF systems cannot provide eight bunches per ring and the transition times of the kickers in the transfer line to the PS are too long to allow such a bunch pattern.

The high energy injector linac, the Superconducting Proton Linac (SPL), would be the ideal solution for this problem and the bunch pattern (see Eq. B.1) could be generated from the source without special difficulties.

B.2 Bunch pattern for the combination of 32 bunches

A simpler solution can be found for the case of 32 bunches. It resembles a scheme presented in [242]. The final bunch pattern in the PS in this case is given by

$$2 \otimes (32 \otimes b \oplus 4 \otimes e) \oplus 12 \otimes e \tag{B.2}$$

and a possible way to generate such a pattern can be sketched as follows (Fig. B.1): Firstly,

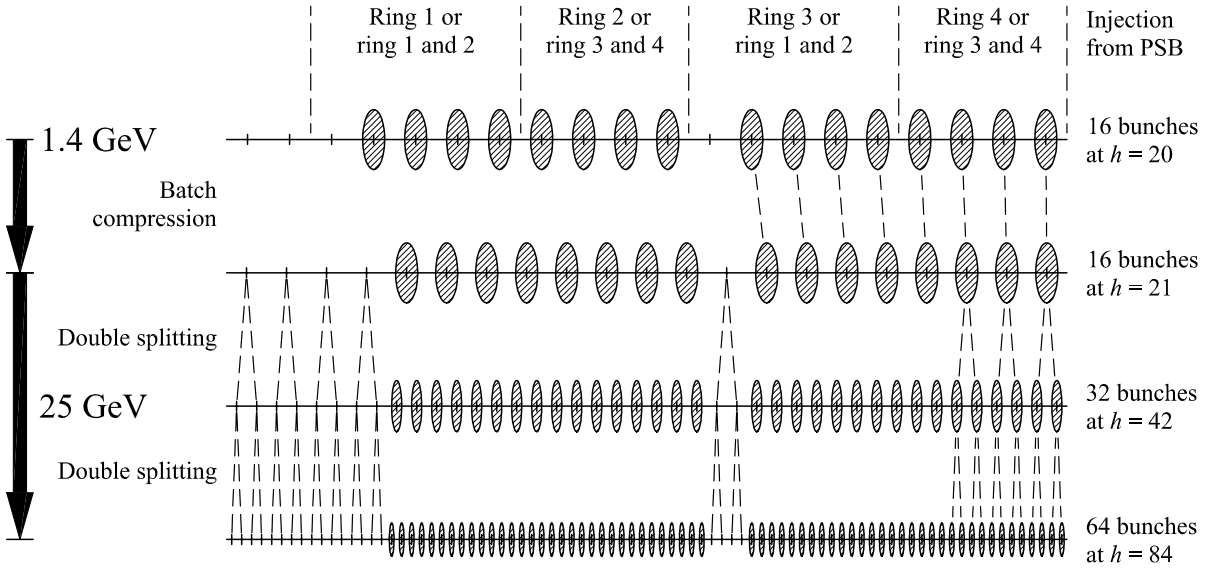

Fig. B.1: Beam preparation scheme to generate trains of 32 bunches with gaps of four empty bucket positions in the PS.

four times four bunches are injected from the booster working at $h = 5$ into matched buckets of the corresponding harmonic in the PS ($h = 20$) in such a way the bunches from two booster rings are stringed up without any gap followed by a gap of one bunch position. Secondly, the harmonic number is adiabatically increased by batch compression to $h = 21$ so that the corresponding bunch pattern becomes

$$2 \otimes (8 \otimes b \oplus 1 \otimes e) \oplus 3 \otimes e\,.$$

Such a pattern can be accelerated with the present 10 MHz main RF system installed in the RF to 26 GeV. Similar to the production of the nominal LHC bunch train, the bunches are finally split twice at the flat-top with existing RF equipment and the resulting bunch pattern corresponds to Eq. (B.2). It is worth noting that the re-combination scheme from the booster also demands shorter kicker rise times than presently available and about 30 ns switching time should be reached between at least two pairs of booster rings. Again in that case, a new injector linac could provide the bunch pattern Eq. (B.2) directly on $h = 21$ without needing the harmonic hand-over from $h = 20$ to 21.

Appendix C

Fast Batch Compression RF Gymnastics in the SIS100

A similar RF manipulation for the combination of bunches as discussed for the long bunch option in the LHC is proposed to be applied in the planned SIS100 of the FAIR project at GSI.

C.1 Introduction

For the physics with radioactive ion beams as well as the plasma physics programme at the GSI future facility (FAIR) it is essential to generate extremely short and intensive ion bunches in the energy range of some 400 MeV/u to 2.7 GeV/u. The largest acceptable bunch length is given by the thermodynamic expansion time of the targets, which is in the order of 50 ns. The accelerator foreseen to produce these bunches is the SIS100 (Schwere-Ionen-Synchrotron) that will have a magnetic rigidity of 100 Tm and a circumference of 1083.6 m which is five times the circumference of its injector, the existing SIS12/18.

In the present stage of planning the SIS12 will deliver four times two bunches to the SIS100. The main RF system of the SIS12 will be operated at the second harmonic of the revolution frequency while the SIS100 will be equipped with an RF system working at the tenth harmonic. Thus, eight bunches will be injected into the SIS100 and accelerated to the desired flat-top energy.

In the design report of the FAIR facility a sophisticated barrier bucket RF gymnastics was suggested to confine these eight bunches to one single bunch and to compress it to its final bunch length in the range of 50 ns by means of fast bunch rotation in the longitudinal phase space [243, 244]. On the one hand, this solution requires a complex and costly barrier bucket RF system. On the other hand, the bunch compression by adiabatically moving barriers in longitudinal phase space takes too long compared to the acceleration time assumed that the emittance blow-up is kept within reasonable limits. Therefore, a new scheme of subsequent batch compression and bunch merging avoiding the disadvantages mentioned above is proposed which is based on the same bunch combination RF gymnastics as the long and flat bunch upgrade option in the LHC. It will be possible to make extensive use of the RF system with which the synchrotron will be equipped for acceleration.

C.2 The batch combination procedure for the SIS100

The heavy ion synchrotron SIS100 will be equipped with an acceleration system based on magnetic alloy or ferrite loaded RF systems covering a frequency range of at least 1.1 to 2.4 MHz (considering that acceleration will take place at harmonic $h = 10$). Such an RF frequency range allows RF manipulations at flat-top energy, e.g. an Uranium U^{28+} beam at 400 GeV/u, between the harmonic numbers $h = 5$ to 10. Furthermore, the RF acceleration system is planned to work at rather high synchronous phase of up to 30 - 40^0 so that at fixed energy even part of its voltage is sufficient to produce bucket areas much larger than the bunch emittances.

Therefore, the following scenario is suggested for the pre-compression of a single intense ion bunch: firstly, four cycles of two bunches each are injected to SIS100 at a kinetic energy of 100 MeV/u. As the SIS100 has five times the circumference of its injector SIS18, there will be two empty buckets, thus only 80 % of the machine is occupied. These bunches are accelerated to flat-top energy and secondly merged to four bunches at $h = 5$. Thirdly, the four bunches are confined to one single bunch using subsequent batch compression and bunch pair merging. Finally one ends up with a single bunch at $h = 5$ which may then be compressed by fast bunch rotation to its desired length of about 50 ns. It is important to point out that additional amplitude modulation during the batch compression as introduced Sec. 5.2.4 is required to preserve sufficient bucket areas along the batch. An overview of bunch patterns and harmonic numbers used during the scheme is given in Tab. C.1. The movement and merging of the

	Bunch pattern	Harmonic numbers
1. Bunch merging	$8 \otimes b \oplus 2 \otimes e \rightarrow 4 \otimes b \oplus 1 \otimes e$	$10 \rightarrow 5$
1. Batch compression	$4 \otimes b \oplus 1 \otimes e \rightarrow 4 \otimes b \oplus 6 \otimes e$	$5 \rightarrow 6 \rightarrow 7 \rightarrow 8 \rightarrow 9 \rightarrow 10$
2. Bunch merging	$4 \otimes b \oplus 6 \otimes e \rightarrow 2 \otimes b \oplus 3 \otimes e$	$10 \rightarrow 5$
2. Batch compression	$2 \otimes b \oplus 3 \otimes e \rightarrow 2 \otimes b \oplus 8 \otimes e$	$5 \rightarrow 6 \rightarrow 7 \rightarrow 8 \rightarrow 9 \rightarrow 10$
3. Bunch merging	$2 \otimes b \oplus 8 \otimes e \rightarrow 1 \otimes b \oplus 5 \otimes e$	$10 \rightarrow 5$
Fast Bunch rotation		2

Tab. C.1: Bunch patterns and harmonic numbers for the proposed batch compression scheme in the SIS100.

buckets during the RF gymnastics is shown in Fig. C.1.

C.2.1 Adiabaticity and emittance development

The RF gymnastics to compress and merge the initial bunches to a single dense bunch should be as fast as possible, whereas longitudinal blow-up should be kept within acceptable limits. Several tracking calculations were done to estimated the expected emittance increase for various time lengths. Figs. C.2 to C.5 show the emittance development for different velocities of the batch compression RF gymnastics.

The initial emittance was assumed to be 8×12.5 eVs (total of all charges, U^{28+}) corresponding to a coasting beam with a momentum spread of $\Delta p/p \simeq 5 \times 10^{-4}$ in the SIS12. The emittance given is calculated by summing up the areas of optimized ellipses containing 99 % of the particles of each bunch. This explains why the calculated emittance may be slightly below the initial assumption. The calculation for the 6 s long procedure is for reference only but demonstrates that the RF gymnastic is indeed very clean when the adiabaticity is well respected. The short emittance growths during the bunch mergings arises because ellipses give insufficient approximations of the bunch distribution; but this is only a numerical effect. The bunch boundary is totally non-elliptic during merging.

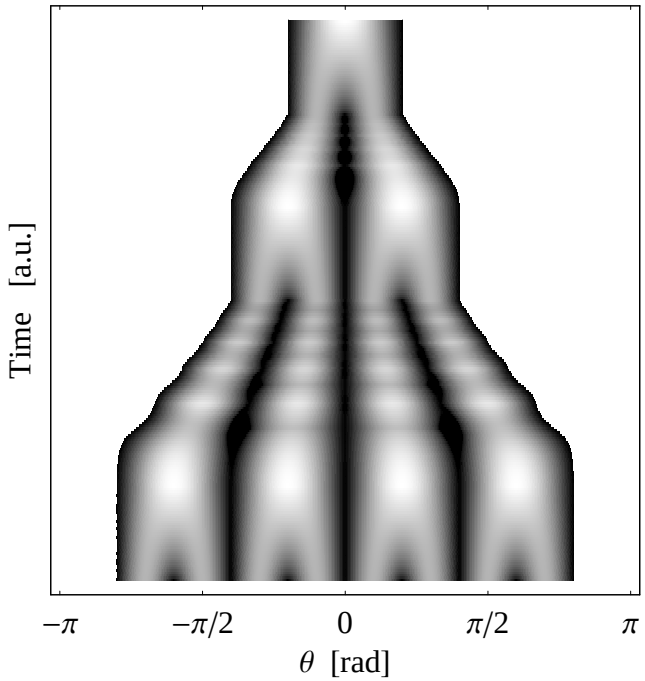

Fig. C.1: Movement and merging of the RF buckets during batch compression in the SIS100. The gray level is proportional to the square root of the energy height of the separatrix at a given θ. White areas signify that there is no occupied bucket.

From these calculation it is visible that even for a batch compression as short as 0.12 s, the emittance blow-up is still acceptable with some 40 %. However, the emittance is much more diluted by an even faster RF gymnastics and the optimum is a trade-off between dilution and time. It is worth noting that beam induced effects, which are neglected so far, may lead to further blow-up especially when the batch compression takes a rather long time. Taking these effects into account may lead to a well defined emittance blow-up minimum.

C.3 Hardware requirements

A main advantage of the proposed RF gymnastics is that only little additional high power RF hardware will be required. The scheme relies heavily on the flexibility of the acceleration system in the SIS100. As mentioned, it will cover the harmonics from 5 to 10 at flat-top and delivering some 400 kV. Thus it matches very well to the requirements of the batch compression procedure.

The RF voltage needed for the main carriers during batch compression is about 100 kV. Therefore, the cavities of the acceleration are split in groups: the first two groups generate both main carriers for the batch hand-over to the next higher harmonic number. A third group contains the same number of cavities but produces no RF voltages as it is tuned and prepared for the next harmonic number. The cavities left will be used to generate the two amplitude modulation carriers. The cyclic operation of the cavity groups is sketched in Fig. C.6, whereas the complete voltage program is shown in Fig. C.7. The grouping of the cavities is proposed such that always one spare group capable of delivering some 100 kV is tuned without amplitude and thus no time is lost due to limitations of the cavity tuning speed.

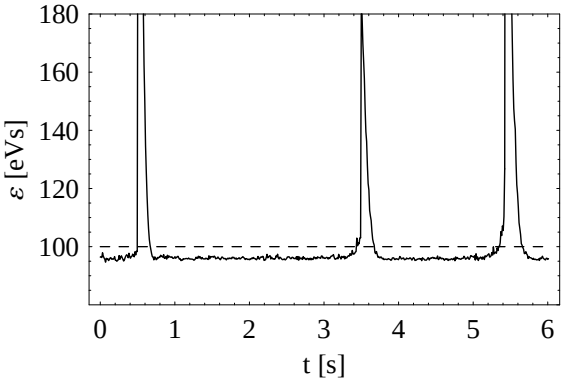

Fig. C.2: Emittance development during the batch compression lasting 6 s.

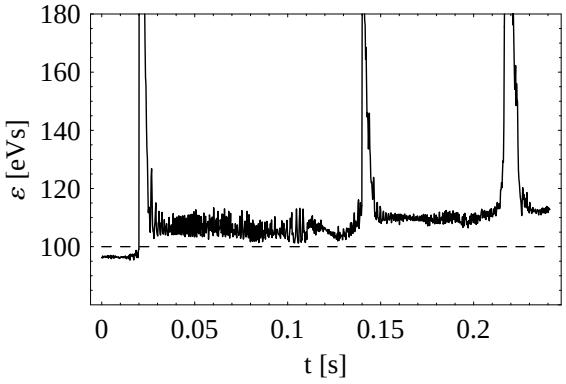

Fig. C.3: Emittance development during the batch compression lasting 240 ms.

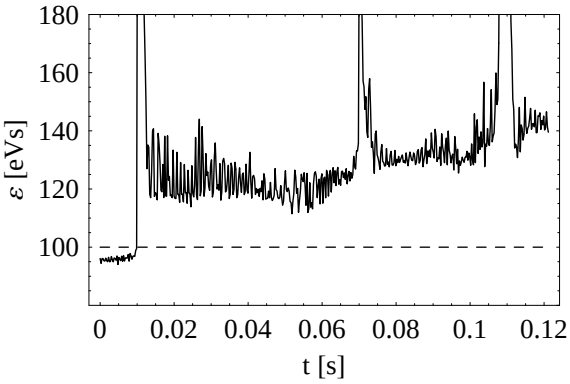

Fig. C.4: Emittance development during the batch compression lasting 120 ms.

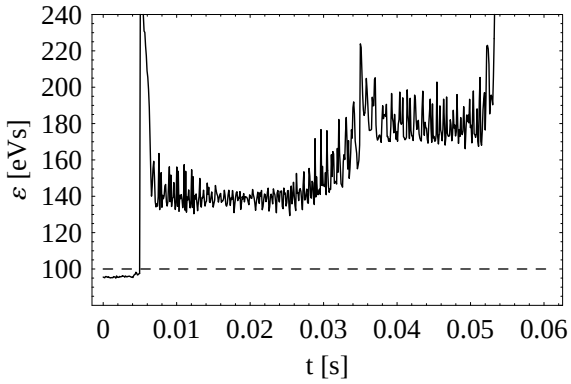

Fig. C.5: Emittance development during the batch compression lasting 60 ms. The vertical scale is different from the other plots.

However, two additional RF systems will be necessary as the equilibrated batch compression needs some 20 kV at $h = 4$ and $h = 11$ during the beginning and the end of the two batch compressions. These two frequencies might not be covered by the main acceleration system. As their voltage is quite moderate and they are only operated at fixed frequencies, the additional costs are much less compared to other schemes [243].

C.4 Conclusions

An RF gymnastics scheme to confine all bunches of an eight bunch batch in the SIS100 by repetitive use of batch compression and bunch merging to a single, dense bunch is proposed and analyzed. This scenario makes extensive use of the acceleration RF system which has to be installed by definition. In addition to the low level RF equipment required to provide flexibility of the acceleration system, only two fixed frequency RF systems at moderate amplitudes have to be installed additionally.

Furthermore, the scheme has several inherent advantages. Firstly, it consists of a chain of conventional RF gymnastics which have been proven at different accelerators to work well up to largest particle intensities. Secondly, the beam is always kept at large RF voltages meaning that RF focusing is strong and the beam can be kept under control of feedback loops if necessary.

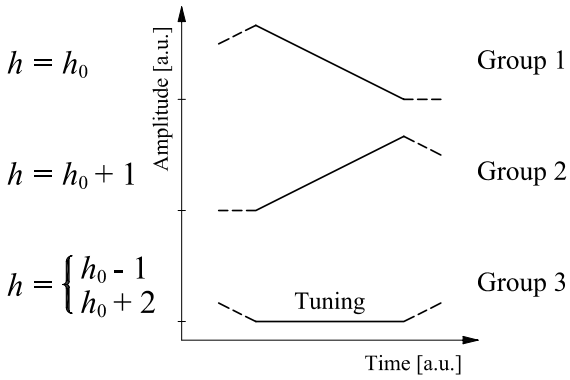

Fig. C.6: Amplitudes of the first three groups of RF cavities. For simplicity the amplitude variations are assumed to be linear. Furthermore, the modulation cavities are not shown.

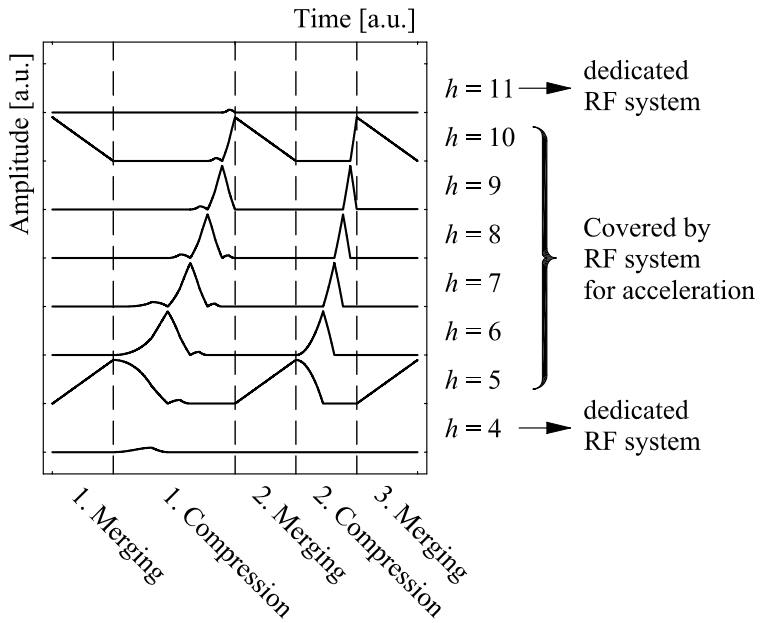

Fig. C.7: Voltage programme for the complete compression RF gymnastics in the SIS100. The amplitudes are normalized to 100 kV. It should be mentioned that no more than four RF systems act on the beam simultaneously. This can be easily achieved by the described grouping of RF cavities. The RF phases are generally fixed but have to be switched by 180^0 for the third bunch merging. The bucket configuration of the voltage programme has been illustrated in Fig. C.1.

Finally, as a consequence of the large RF amplitudes, the proposed scenario can be executed within 0.12 s, while the longitudinal emittance blow-up caused by dilution stays reasonable. This amount of time required at flat-top energy is not negligible but at least comparable to the duration of the acceleration (0.1–0.2 s, [245]).

It should be mentioned that collective effects caused high beam current are not covered here and should be investigated elsewhere. Especially direct space charge is supposed to limit the performance at low extraction energies. Flat-topping [246] or hollow bunch techniques [247] could be added for improvement. However, a good candidate for a scheme to perform the bunch pre-compression in the SIS100 is found and should be analyzed in more detail. In the case of an RF acceleration system working at the 20th harmonic, a similar scheme could be applied, but the bucket area of such a system would not be sufficient to end up with a single bunch. Additional RF installations would be necessary.

The investigation of different scenarios for the final bunch compression indicates that the RF acceleration system can be utilized to optimize the synchrotron frequency distribution for linearization during bunch rotation. Approximately 1.5 times more particles, some 80 % of the bunch, are transported to the desired target emittance ellipse ($\tau = 50\,\mathrm{ns}$, $\Delta p/p = 0.01$). Finally, the possibility of a staged installation of the RF systems in SIS100 should be considered. Even without the very costly bunch rotation system bunches with some 150 ns length can be obtained.

Appendix D

Synchrotron Frequency in an Accelerating Bucket

The synchrotron frequency distribution of particles oscillating in the longitudinal phase space of a stationary bucket has been derived in Sec. 2.2.6. The calculation is extended to the general case of particles in a single harmonic accelerating bucket in what follows. The order of the approximations is chosen so that the first term which is dependent on ϕ_0 is kept.

The Hamiltonian of motion for the interaction of particles with one RF system is given by Eq. (2.20)

$$H(\Delta\phi, \dot{\phi}) = \frac{1}{2}\dot{\phi}^2 + \frac{\omega_s^2}{\cos\phi_0}[\cos\phi_0 - \Delta\phi\sin\phi_0 - \cos(\phi_0 + \Delta\phi)]\,. \tag{D.1}$$

Replacing the trigonometric expressions by their Taylor expansion up to fourth order in $\Delta\phi$ and division by the constant factor $h\eta\omega_0$ leads to [248]

$$H\left(\Delta\phi, \frac{\Delta p}{p}\right) = \frac{1}{2}h\omega_0\eta\left(\frac{\Delta p}{p}\right)^2 + \frac{1}{2}\frac{\omega_0}{h\eta}Q_s^2\left[\Delta\phi^2 - \frac{1}{6}\Delta\phi^3\tan\phi_0 - \frac{1}{12}\Delta\phi^4 + \ldots\right], \tag{D.2}$$

where $Q_s = \omega_s/\omega_0$ denotes the synchrotron tune.

The Hamiltonian can be converted to a new set of so-called action-angle variables by applying the transformation function (see e.g. [249])

$$F_1(\Delta\phi, \psi) = -\frac{Q_s}{2h|\eta|}\Delta\phi^2\tan\psi\,.$$

According to the transformation equations

$$J = -\frac{\partial F_1}{\partial\psi} = \frac{Q_s}{2h|\eta|}\Delta\phi^2\frac{1}{\cos^2\psi} \qquad \text{and} \qquad \frac{\Delta p}{p} = -\frac{Q_s}{h|\eta|}\Delta\phi\tan\psi \tag{D.3}$$

the old set of variables is expressed by

$$\Delta\phi = \sqrt{\frac{2h|\eta|J}{Q_s}}\cos\psi \qquad \text{and} \qquad \frac{\Delta p}{p} = -\sqrt{\frac{2Q_sJ}{h|\eta|}}\sin\psi\,.$$

After some algebraic transformations the Hamiltonian can be rewritten as

$$H(\psi, J) = \omega_0Q_sJ - \frac{1}{12}\omega_0\sqrt{h|\eta|Q_s}\tan\phi_0J^{3/2}(\cos 3\psi + 3\cos\psi) - \frac{1}{6}\omega_0h|\eta|J^2\cos^4\psi\,, \tag{D.4}$$

where the relation $\cos^3\psi = (\cos 3\psi + 3\cos\psi)/4$ has been used. The next step is the removal of the terms proportional to $J^{3/2}$ by application of the canonical perturbation theory [250]. Choosing

$$F_2(\psi, I) = \psi I + G_3(I)\sin 3\psi + G_1(I)\sin\psi \tag{D.5}$$

as general attempt for a generating function to convert the action J into a new action-angle variable I [248], the transformation equation simply becomes

$$J = \frac{\partial F_2}{\partial \psi} = I + 3G_3(I)\cos 3\psi + G_1(I)\cos\psi\,.$$

This expression is inserted into the Hamiltonian and the functions $G_1(I)$ as well as $G_3(I)$ are calculated so that terms proportional to $I^{3/2}$ vanish. To get the conditional equations it is thus sufficient to keep only orders below I^2:

$$\begin{aligned} H(\psi, I) = \omega_0 Q_s I + 3\omega_0 Q_s G_3(I)\cos 3\psi + \omega_0 Q_s G_1(I)\cos\psi \\ - \frac{1}{12}\omega_0\sqrt{2h|\eta|Q_s}\tan\phi_0 I^{3/2}(\cos 3\psi + 3\cos\psi) + \mathcal{O}(I^2)\,. \end{aligned} \tag{D.6}$$

Now it becomes clear that the choice of the generating function Eq. (D.5) is reasonable and the conditional equations for $G_1(I)$ and $G_3(I)$ become

$$\begin{aligned} \left(\omega_0 Q_s G_1(I) - \frac{1}{4}\sqrt{2h|\eta|Q_s}\tan\phi_0 I^{3/2}\right)\cos\psi &= 0 \\ \text{and} \quad \left(3\omega_0 Q_s G_3(I) - \frac{1}{12}\sqrt{2h|\eta|Q_s}\tan\phi_0 I^{3/2}\right)\cos 3\psi &= 0 \end{aligned}$$

so that the functions can be written as

$$G_1(I) = \frac{1}{4}\sqrt{\frac{2h|\eta|}{Q_s}}\tan\phi_0 I^{3/2} \quad \text{and} \quad G_3(I) = \frac{1}{36}\sqrt{\frac{2h|\eta|}{Q_s}}\tan\phi_0 I^{3/2}\,. \tag{D.7}$$

The general transformation equation (D.5) reduces to

$$J = I + \frac{1}{12}\sqrt{\frac{2h|\eta|}{Q_s}}\tan\phi_0 I^{3/2}(\cos 3\psi + 3\cos\psi)\,. \tag{D.8}$$

To insert this result into the Hamiltonian Eq. (D.4) powers of J with a precision up to an order of I^2 have to be derived according to

$$\begin{aligned} J &= I(1 + aI^{1/2}) \\ J^{3/2} &= I^{3/2}\left(1 + \frac{3}{2}aI^{1/2}\right) + \mathcal{O}(I^{5/2}) \\ J^2 &= I^2(1 + aI^{1/2} + a^2 I) = I^2 + \mathcal{O}(I^{5/2}) \end{aligned}$$

so that the Hamiltonian including perturbation orders up to $\mathcal{O}(I^2)$ can be rewritten as

$$H(\psi, I) = \omega_0 Q_s I - \frac{1}{6}\omega_0 h|\eta|I^2\cos^4\psi - \frac{1}{3}\omega_0 h|\eta|I^2\tan\phi_0\cos^6\psi\,. \tag{D.9}$$

For the calculation of the oscillating frequency the knowledge of the averaged Hamiltonian over one oscillation period in ψ is sufficient and according to

$$< \cos^4 \psi >= \frac{3}{8} \qquad \text{and} < \cos^6 \psi >= \frac{5}{16}$$

the averaged Hamiltonian

$$< H(I,\psi) > = < H > = \omega_0 Q_s I - \frac{1}{16}\omega_0 h|\eta| \left(1 + \frac{5}{3}\tan^2\phi_0\right) I^2 \tag{D.10}$$

is obtained.

As introduced in Sec. 2.2.6 the synchrotron frequency can be derived directly from the Hamiltonian in action-angle variables, namely

$$\omega(I) = \frac{\partial < H >}{\partial I} = \omega_0 Q_s \left[1 - \frac{h|\eta|}{8Q_s}\left(1 + \frac{5}{3}\tan^2\phi_0\right) I\right] . \tag{D.11}$$

Now the action-angle variable I remains to be converted back to phase space coordinates. With respect to the set of canonical transformations Eq. (D.3) applied to the Hamiltonian, the action-angle variable ψ vanishes in case of an oscillating test particle reaching its maximum phase excursion at $\Delta\phi_m = \sqrt{2h|\eta|J/Q_s}$. Up to the first leading order the second transformation just gives $J \simeq I$ so that

$$I \simeq \frac{Q_s}{2h|\eta|}\Delta\phi_m^2 .$$

Finally, the dependence of the synchrotron frequency on the maximum phase excursion $\Delta\phi_m$ can be written as [33, 251]

$$\frac{\omega(\Delta\phi_m)}{\omega_s} \simeq 1 - \frac{1}{16}\left(1 + \frac{5}{3}\tan^2\phi_0\right)\Delta\phi_m^2 , \tag{D.12}$$

which is identical to Eq. (2.44).

It is worth noting that some authors use slightly different relations which might be based on other approximations of the Hamiltonian, see e.g. [206, 252].

Appendix E

Derivation of Betatron Tune Shifts

Forces acting focusing or defocusing can be generally approximated as an additional element in the machine lattice which shifts the betatron frequencies of a circular accelerator. This interpretation is independent of whether the forces have their origin in real quadrupole magnets, in self-field of the beam, like in the case of space-charge, or in field generated by a counter-rotating beam. In what follows, it is assumed that both transverse phase space planes are well decoupled so that the derivation can be simplified to one transverse direction only.

It can be shown from the general solution of the transverse particle motion in connection with the condition for periodicity from one turn to the next that the transformation matrix for the a particle with the initial offset x at its local derivation $x' = dx/dz$ can be written as [253]

$$\begin{pmatrix} x \\ x' \end{pmatrix}_{z_0+2\pi R} = M_{z_0 \to z_0+2\pi R} \begin{pmatrix} x \\ x' \end{pmatrix}_{z_0} \quad \text{with}$$

$$M_{z_0 \to z_0+2\pi R} = \begin{pmatrix} \cos 2\pi Q + \alpha_0 \sin 2\pi Q & \beta_0 \sin 2\pi Q \\ -\gamma_0 \sin 2\pi Q & \cos 2\pi Q - \alpha_0 \sin 2\pi Q \end{pmatrix} , \quad \text{(E.1)}$$

where Q is the number of betatron oscillations per revolution and β_0, $\alpha_0 = -\beta'|_{z=z_0}/2$ as well as $\gamma_0 = (1+\alpha_0^2)/\beta_0$ are the optical functions at the position z_0 of the perturbation. The transverse beam dimension is proportional to $\sqrt{\beta(z)}$. The transformation matrix of a quadrupole acts only on the beam divergence and is given by

$$M_{\mathrm{Q}} = \begin{pmatrix} 1 & 0 \\ -kl & 1 \end{pmatrix} . \quad \text{(E.2)}$$

The length of the quadrupole in z-direction is defined by l and its so-called strength[1] is k in units of $[k] = 1/\mathrm{m}^2$. The quadrupole strength is defined for a magnetic field that vanishes at the beam center and that grows linearly with the distance (see Sec. 4.2.2):

$$k_x = \frac{e}{p}\frac{dB_y^{\mathrm{quad}}}{dx} = -\frac{1}{m_0\gamma\beta^2c^2}\frac{dF_x}{dx} \quad \text{and} \quad k_y = -\frac{1}{m_0\gamma\beta^2c^2}\frac{dF_y}{dy} . \quad \text{(E.3)}$$

It is worth noting that k_x and k_y are coupled for a quadrupole magnet [255] so that $k_x = -k_y = k$, which e.g. is not the case for beam-beam forces. The definitions above show that focusing or defocusing forces acting on the beam can be expressed by a short quadrupole at $z = z_0$ with

[1] The sign of the quadrupole strength is not unique in the literature, e.g. compare [253, 254].

length dz and Δk as its quadrupole strength. This additional element has to be added to the transformation matrix Eq. (E.1) so that the perturbed transformation for one turn becomes

$$M^{\text{pertub}}_{z_0+2\pi R} = \begin{pmatrix} 1 & 0 \\ -\Delta k\, ds & 1 \end{pmatrix} M_{z_0+2\pi R} \tag{E.4}$$

$$= \begin{pmatrix} \cos 2\pi Q + \alpha_0 \sin 2\pi Q & \beta_0 \sin 2\pi Q \\ -\Delta k\, dz\, (\cos 2\pi Q + \alpha_0 \sin 2\pi Q) & -\Delta k\, dz\, \beta_0 \sin 2\pi Q \\ -\gamma_0 \sin 2\pi Q & +\cos 2\pi Q - \alpha_0 \sin 2\pi Q \end{pmatrix} \tag{E.5}$$

which can be expressed in the form of an unperturbed transformation matrix with modified betatron tune:

$$M_{z_0+2\pi R}(Q+dQ) = \begin{pmatrix} \cos 2\pi(Q+dQ) & \beta_1 \sin 2\pi(Q+dQ) \\ +\alpha_1 \sin 2\pi(Q+dQ) & \\ -\gamma_1 \sin 2\pi(Q+dQ) & \cos 2\pi(Q+dQ) \\ & -\alpha_1 \sin 2\pi(Q+dQ) \end{pmatrix} . \tag{E.6}$$

The new optical functions α_1, β_1 and γ_1 also vary due to the perturbing quadrupole as an additional optical element.

Comparing Eq. (E.5) and (E.6) all matrix elements must be equal in general. For the derivation of the betatron tune only, it is however sufficient to compare the traces of the matrices [256, 257] so that relation between the perturbing quadrupole element parameters $\Delta k\, dz$ and the tune shift can be written as

$$2\cos 2\pi Q - \Delta k\, dz\, \beta_0 \sin 2\pi Q = 2\cos 2\pi(Q+dQ)\,,$$

and for $dQ \ll 1$ it reduces to

$$\Delta k\, dz\, \beta_0 = 4\pi\, dQ\,. \tag{E.7}$$

Finally, the finite tune shift is calculated by integration of Eq. (E.7) with respect to a beta function $\beta(z)$ that may vary along the quadrupolar perturbation:

$$\Delta Q = \frac{1}{4\pi} \int \Delta k(z) \beta(z)\, dz\,. \tag{E.8}$$

This result corresponds to Eq. (4.39).

Appendix F

The Direct Space Charge Tune Spread

The direct space charge tune spread which is regarded as an ultimate intensity limit for low and intermediate energy accelerators can be derived similarly to the calculation of the beam-beam tune spread as shown in Sec. 4.2. Firstly, the focusing or defocusing electromagnetic force is calculated, which is secondly transformed to a transverse tune shift[1] (see App. E).

In the most simple case of a long and round beam the transverse electric field and the magnetic induction outside the beam can be expressed by

$$E_x = \frac{I}{\pi\epsilon_0\beta c}\cdot\frac{x}{a_x(a_x+a_y)}\,, \qquad E_y = \frac{I}{\pi\epsilon_0\beta c}\cdot\frac{y}{a_y(a_x+a_y)}$$

and

$$B_x = -\frac{\mu_0 I}{\pi}\cdot\frac{y}{a_y(a_x+a_y)}\,, \qquad B_y = \frac{\mu_0 I}{\pi}\cdot\frac{x}{a_x(a_x+a_y)}\,,$$

where a_x and a_y denote the transverse radii of the elliptic beam. The transverse components of the Lorentz force for a round beam with $a = a_x = a_y$ thus become

$$F_x = \frac{eE_x}{\gamma^2} = \frac{eI}{2\pi\epsilon_0\beta\gamma^2 c}\cdot\frac{x}{a}^2 \qquad \text{and} \qquad F_y = \frac{eE_y}{\gamma^2} = \frac{eI}{2\pi\epsilon_0\beta\gamma^2 c}\cdot\frac{y}{a}^2\,. \tag{F.1}$$

Transforming these forces to tune shifts according to Eq. (E.8), reduces the direct space charge tune shift to

$$\Delta Q = \frac{eI}{8\pi^2 m_0\beta^3\gamma^3 c^3\epsilon_0}\oint\frac{\beta(z)}{a(z)^2}\,dz\,. \tag{F.2}$$

It should be mentioned that the tune shift also can be calculated directly from Hill's equation of betatron motion [259]. As the beam radius $a(z)$ is proportional to the square root of the beta function numerator and denominator of the integrand have an identical dependence on z so that the integral may be expressed in terms of an averaged beta function: $2\pi R<\beta>/a^2$. Furthermore, the betatron function in the tune integral is replaced by average value over one turn according to

$$Q = \frac{1}{2\pi}\oint\frac{1}{\beta(z)}\,dz = \frac{R}{<\beta>}$$

[1] According to the analysis in [258] the incoherent space charge tune shift is also known as Laslett tune shift.

so that the tune shift can be written as

$$\Delta Q = \frac{eIR^2}{4\pi m_0 \beta^3 \gamma^3 c^3 \epsilon_0 Q a^2} \,. \tag{F.3}$$

Introducing the normalized transverse beam emittance $\varepsilon_n = a^2 Q/R$ and converting the current to the particle intensity $I = Ne\beta c/(2\pi R)$, which both remain constant throughout the acceleration, the tune spread finally reduces to

$$\Delta Q = \frac{Ne^2}{8\pi^2 \epsilon_0 \beta \gamma^2 m_0 c^2 \varepsilon_n} \,, \tag{F.4}$$

where its energy dependence proportional to $1/(\beta\gamma^2)$ becomes directly obvious.

It is worth noting that Eq. (F.4) is only the most simple case of the incoherent space charge tune shift. As the beam normally travels inside a metallic beam pipe, field corrections due to multiple image currents must be taken into account [260]. Additional geometrical corrections to different shapes of vacuum chamber and beam have to be added to Eq. (F.4) in the case of elliptic beams in a non-circular beam pipe [258].

List of Symbols

Symbol	Quantity	Unit
α	adiabaticity	–
α	inverse cavity filling time $\omega_r/(2Q)$	[1/s]
α	normalized energy separation for slip-stacking	–
α_c	momentum compaction factor, $1/\gamma_{\mathrm{tr}}$	–
$\alpha(\phi_0)$	bucket area reduction function	–
β	velocity relative to the speed of light, v/c	–
β	moving barrier bucket adiabaticity coefficient	–
β^*	betatron amplitude function at the interaction point	[m]
$\beta(z)$	betatron amplitude function	[m]
γ	ratio of total and rest mass	–
γ_{tr}	γ at transition energy	–
ϵ_0	vacuum permittivity, $8.854187817 \cdot 10^{-12}\,\mathrm{A\,s/(V\,m)}$	[A s/(V m)]
ε_0	initial longitudinal emittance	[eV s]
ε_l, $\varepsilon_{\mathrm{RMS}}$	longitudinal (RMS) emittance	[eV s]
ε_n	normalized transverse emittance	[m rad]
ζ	normalized longitudinal distribution	–
η	phase slip factor, $\alpha - 1/\gamma^2$	–
θ	particle phase with respect to the accelerator	[rad]
θ	full crossing angle	[rad]
$\lambda(\phi)$, $\lambda(z)$	normalized line density	[1/rad], [1/m]
μ_0	vacuum permeability, $4\pi \cdot 10^{-7}\,\mathrm{V\,s/(A\,m)}$	[V s/(A m)]
σ_x, σ_y, σ_z	beam dimensions	[m]
σ^*	transverse RMS beam dimension at the interaction point	[m]
ς	cross section	[m^2]
τ, $2\hat{\tau}$	total bunch duration	[s]
τ_{bc}, τ_{bm}	duration of batch compression, bunch merging	[s]
τ_{sep}	bunch spacing	[s]
$1/\tau$	instability growth rate	[1/s]
ϕ	particle phase with respect to RF phase	[rad]
ϕ_0	synchronous phase	[rad]
ϕ_l, ϕ_u	phase limits of a trajectory	[rad]
$\Delta\phi_l$, $\Delta\phi_u$	phase limits with respect to synchronous phase	[rad]
$\Delta\phi_m$	phase limits of a symmetric trajectory	[rad]
$\chi_{\mathcal{L}}$	luminosity form factor	–
ω	$2\pi \cdot$ frequency	[rad/s]
ω_0	$2\pi \cdot$ revolution frequency	[rad/s]

ω_r	$2\pi \cdot$ resonance frequency	[rad/s]
ω_s	$2\pi \cdot$ synchrotron frequency	[rad/s]
A, A_{eVs}	bucket area	[J s], [e Vs]
B	magnetic induction	[T]
c	speed of light in vacuum, 299792458 m/s	[m/s]
c_{sf}	space charge parameter	–
$D(\alpha\tau_{\mathrm{sep}})$	beam cavity coupling form factor	–
E	energy	[J], [eV]
E_x, E_r	electric field	[V/m]
E_0	energy of the reference particle	[J], [eV]
$\Delta\hat{E}$	bucket height	[J], [eV]
e	electron charge, $1.602177 \cdot 10^{-19}$ C	[C]
F	form factor of the order of unity	–
$\vec{F}_L$	Lorentz force, $e(\vec{E} + \vec{v} \times \vec{B})$	[N]
$F_0(x)$	fully normalized energy distribution	–
$F_m(2\omega_r\hat{\tau})$	bunch distribution form factor	–
f_0	revolution frequency	[Hz]
$f(\phi, \dot{\phi})$	normalized longitudinal distribution	[1/J]
$f(\theta, E)$	longitudinal beam distribution	[1/J]
$f_0(E)$	unperturbed beam energy distribution	[1/J]
$f_1(E)$	perturbation of the energy distribution	[1/J]
$f_0(\tau, \Delta E, z)$	longitudinal bunch distribution	[1/(J s)]
$f_0(\tau, \Delta E)$	unperturbed bunch distribution	[1/(J s)]
$f_1(\tau, \Delta E, z)$	perturbation of the bunch distribution	[1/(J s)]
f_b	harmonic weight form factor, two for short bunches	–
$\mathrm{fs_{PS}}$, $\mathrm{fs_{LHC}}$	filling scheme in the PS, LHC	–
$g(\phi)$	normalized RF amplitude function	–
$g(\theta, \Delta E/\omega)$	longitudinal beam distribution	[1/(rad J s)]
$g_0(r)$	normalized radial distribution	[1/s^2]
H	Hamiltonian, unit depends on normalization	(various)
h	harmonic number of the RF system	–
h_b	local harmonic number of barrier RF pulse	–
I, I_0	beam current	[A]
I	normalized action-angle variable	–
I_g, I_r, I_b	generator, resonator, harmonic beam current	[A]
$J(H)$	action-angle variable, unit depends on normalization	–
$J_m(x)$	Bessel function of the first kind	–
$K(x)$	complete elliptic integral of the first kind	–
k, k_x, k_y	quadrupole strength	[m]
$\mathcal{L}$	bunch crossing luminosity	[cm^{-2}s^{-1}]
$\mathcal{L}_{\mathrm{tot}}$	total luminosity	[cm^{-2}s^{-1}]
L	circumference of an orbit trajectory	[m]
l_b	total bunch length of a rectangular bunch	[m]
l_{det}	detector length	[m]
M	number of possible coupled bunch modes	–
$M_{z_1 \to z_2}$	beam optics transformation matrix	(matrix)
m	particle rest mass	[kg]

m	coupled bunch mode number	–
m_p	proton rest mass, $938.272\,\mathrm{MeV}/c^2 = 1.67262 \cdot 10^{-27}\,\mathrm{kg}$	[kg]
n	single bunch mode number	–
n_1, n_2	particle density	$[1/\mathrm{m}^3]$
n_b	number of bunches	–
N	particle number	–
dN/dt	interaction rate	[1/s]
p	particle momentum	[kg m/s], $[\mathrm{eV/c}^2]$
Q, Q_0, Q_g	quality factor, unloaded and external	–
Q_x, Q_y	horizontal, vertical betatron tune	–
ΔQ_x, ΔQ_y	betatron tune shift, spread	–
ΔQ_{tot}	total tune shift of two alternate crossings	–
R_{mag}	bending radius of the dipole magnets	[m]
R_{mean}, R	average radius, circumference/(2π)	[m]
R_s	shunt impedance of a resonator	[Ω]
R/Q	characteristic cavity impedance	[Ω]
r_p	classical proton radius, $1/(4\pi\epsilon_0 c^2)e^2/m_p \simeq 1.535 \cdot 10^{-18}\,\mathrm{m}$	[m]
t	time	[s]
$t_1(t)$	time equilibration function	[s]
S	half relative momentum spread at half height	[1/s]
U	RF voltage	[V]
v	velocity	[m/s]
W_0	energy loss or gain of the synchronous particle	[J], [eV]
$W(\phi)$	normalized RF potential function	–
Z	impedance	[Ω]
Z_0	vacuum impedance, $\sqrt{\mu_0/\epsilon_0} \simeq 377\,\Omega$	[Ω]
$Z_\parallel$	longitudinal broad band coupling impedance	[Ω]
$(Z_\parallel/n)_{\mathrm{eff}}$	effective longitudinal broad band impedance	[Ω]
z	longitudinal coordinate	[m]

The physical units in the figures and tables throughout this report are given in square brackets.

Bibliography

[1] V. E. Barnes, P. L. Connolly, D. J. Crennell, B. B. Culwick et al., *Observation of a Hyperon with Strangeness Minus Three*. Phys. Rev. Lett., Vol. 12, 1964, p. 204-206

[2] G. Arnison, A. Astbury, B. Aubert, C. Bacci et al., *Experimental Observation of Isolated Large Transverse Energy Electrons with Associated Missing Energy at* $\sqrt{s} = 540\,GeV$. Phys. Lett., Vol. 122B, 1983, pp. 103-116

[3] F. Abe, M. G. Albrow, S. R. Amendolia, D. Amidei et al., *Evidence for Top Quark Production in* $p\bar{p}$ *Collisions at* $\sqrt{s} = 1.8\,TeV$. FERMILAB-PUB-94/097-E, CDF/PUB/-TOP/PUBLIC/2561, Phys. Rev. D, Vol. 50, 1994, pp. 2966-3026

[4] J. Ellis, *The 115 GeV Higgs Odyssey*. CERN-TH/2003-307, CERN, Geneva, Switzerland, 2000

[5] V. Ruhlmann-Kleider, *Review of Higgs Boson Searches at LEP*. DAPNIA-04-81, Advanced Studies Inst. - Phys. at LHC, Prague, Tcheque Republic, 2003, in: Czechoslovak Journal of Phys., Vol. 54, Suppl. A, 2004, pp. A23-A34

[6] M. Jacob, K. Johnsen, *A Review of Accelerator and Particle Physics at the CERN Intersecting Storage Rings*. CERN 84-13, CERN, Geneva, Switzerland, 1984

[7] V. Hatton, *Operational History of the SPS Collider 1981-1990*. Part. Acc. Conf., San Francisco, California, 1991, pp. 2952-2954

[8] V. Shiltsev for the Collider Run II Team, *Status of Tevatron Collider Run II and Novel Technologies for Luminosity Upgrades*. Europ. Part. Acc. Conf., Lucerne, Switzerland, 2004, pp. 239-243

[9] R. Johnson, *Initial Operation of the Tevatron Collider*. Part. Acc. Conf., Washington, D.C., 1987, pp. 8-12

[10] M. Curch, *Tevatron Run II Performance and Plans*. Europ. Part. Acc. Conf., Paris, France, 2002, pp. 11-14

[11] E. Ciapala, *Stacking and Phase Displacement Acceleration*. CERN 85-19, CERN Acc. School on General Acc. Phys., Gif-sur-Yvette, France, 1984, pp. 195-225

[12] G. Brianti (ed.), Kurt Hübner (ed.), *The Large Hadron Collider in the LEP Tunnel*. CERN 87-05, CERN, Geneva, Switzerland, 1987

[13] The LHC Study Group, *Design Study of the Large Hadron Collider (LHC)*. CERN 91-03, CERN, Geneva, Switzerland, 1991

[14] P. Lefèvre (ed.), T. Petterson (ed.), D. Boussard, L. Evans et al., *LHC, The Large Hadron Collider*. CERN/AC/95-05 (LHC), CERN, Geneva, Switzerland, 1995

[15] O. Brüning, P. Collier, P. Lebrun, S. Myers et al., *LHC Design Report, Volume I, The LHC Main Ring*. CERN-2004-003, CERN, Geneva, Switzerland, 2004

[16] K. Takayama, J. Kishiro, M. Sakuda, Y. Shimosaki et al., *Superbunch Hadron Colliders*. Phys. Rev. Lett., Vol. 88, pp. 144801, 2002

[17] T. Suzuki, *Equations of Motion and Hamiltonian for Synchrotron Oscillations and Synchro-Betatron Coupling*. KEK Report 96-10, KEK, Tsukuba, Japan, 1996

[18] T. Suzuki, *Orbit Theory for Accelerators*. Asian Part. Acc. Conf., Beijing, China, 2001, pp. 463-465

[19] H. Bruck, *Accélérateurs Circulaires de Particules*. Institut National des Sciences et Techniques Nucléaires, Saclay, Presses Universitaires de France, Paris, 1966, p. 165

[20] H. Bruck, *Circular Particle Accelerators*. LA-TR-72-10 Rev., Los Alamos Scientific Laboratory, Los Alamos, New Mexico, 1972, English translation of [19], p. 173

[21] B. W. Montague, *Single-Particle Dynamics - RF Acceleration*. CERN 77-13, 1st Course of the Int. School on Part. Acc. Phys., Erice, Italy, 1976, pp. 63-81

[22] W. Pirkl, *Longitudinal Beam Dynamics*. CERN 95-06, CERN Acc. School on Advanced Acc. Phys., Rhodes, Greece, 1993, pp. 233-257

[23] K. Johnsen, *Effects of Non-Linearities on the Phase Transition*. CERN Symposium on High Energy Acc., CERN, Geneva, Switzerland, 1956, pp. 106-109

[24] H. G. Hereward, *What are the Equations for the Phase Oscillations in a Synchrotron?* CERN 66-6, CERN, Geneva, Switzerland, 1966

[25] V. E. Veksler, *A New Method of Accelerating Relativistic Particles*. Comptes Rendus (Dokaldy) de l'Academie Sciences de l'URSS, Vol. 43, 1944, pp. 329-331

[26] E. M. McMillan, *The Synchrotron - A Proposed High Energy Accelerator*. Phys. Rev., Vol. 68, 1945, pp. 143-144

[27] K. R. Symon, A. M. Sessler, *Methods of Radio Frequency Acceleration in Fixed Field Accelerators with Applications to High Current and Intersecting Beam Accelerators*. CERN Symposium on High Energy Acc., CERN, Geneva, Switzerland, 1956, pp. 44-58

[28] E. Ciapala, S. Myers, C. Wyss, *Phase Displacement Acceleration of High Intensity Stacks in the CERN ISR*. Part. Acc. Conf., Chicago, Illinois, 1977, pp. 1431-1433

[29] H. Damerau, M. Kirk, Y. Liu, *Maschinenexperimente zum longitudinalen Strahlverhalten während des Hochfrequenzeinfangs*. SIS28062.HF, GSI Darmstadt, Germany, 2002

[30] A. A. Andronow, C. E. Chaikin, *Theory of Oscillations*. Princeton, New Jersey, 1949, pp. 75-78

[31] H. Goldstein, *Classical Mechanics*. Addison-Wesley, Reading, Massachusetts, 2nd ed., 1985, pp. 457-461

[32] see [31], pp. 506-509

[33] B. Zotter, *Longitudinal Stability of Bunched Beams, Part II: Synchrotron Frequency Spread*. CERN SPS 81/19 (DI), CERN, Geneva, Switzerland, 1981

[34] B. Zotter, *Sacherer Formulae*. In: A. W. Chao (ed.), M. Tigner (ed.), *Handbook of Accelerator Physics and Engineering*. World Scientific, Singapore, Singapore, 1998, pp. 122-124

[35] A. G. Ruggiero, *Beam Stacking with Suppressed Buckets in the ISR*. CERN 68-22, CERN, Geneva, Switzerland, 1968

[36] K. Takayama, J. Kishiro, K. Koseki, E. Nakamura et al., *Superbunch Acceleration and its Applications*. Europ. Part. Acc. Conf., Paris, France, 2002, pp. 998-1000

[37] C. M. Bhat, *Barrier RF Systems in Synchrotrons*. Europ. Part. Acc. Conf., Lucerne, Switzerland, 2004, pp. 236-238

[38] J. E. Griffin, C. Ankenbrandt, J. A. MacLachlan, A. Moretti, *Isolated Bucket RF Systems in the Fermilab Anitproton Facility*. IEEE Trans. Nucl. Sci., Vol. NS-30, 1983, pp. 3502-3504

[39] A. M. Farson, *The Missing Bucket System*. CERN-ISR-RF-70-27, CERN, Geneva, Switzerland, 1970

[40] L. L. Foldy, *A Method for Expanding the Phase-Stable Regime in Synchronous Accelerators*. Il Nuovo Cimento, Vol. 19, 1961, pp. 1116-1120

[41] J. Claus, M. Month, *Exotic RF Systems for High Intensity High Energy Proton Storage Rings*. BNL 50469, ISA 75-12, Brookhaven Nat. Lab., Upton, New York, 1975

[42] S. Y. Lee, K. Y. Ng, *Particle Dynamics with Barrier RF Systems*. FERMILAB-Pub-96/403, Phys. Rev. E, Vol. 55, 1997, pp. 5992-6001

[43] C. M. Bhat, K. Y. Ng, *Potential-Well Distortion in Barrier RF*. FERMILAB-Conf-03/395-T, e^+e^- Factories 2003, Stanford, California, 2003, pp. WGB02

[44] J. A. MacLachlan, *Longitudinal Tracking With Space Charge and Inductive Wall Coupling Impedance*. FERMILAB-FN-446, Fermi National Accelerator Lab., Batavia, Illinois, 1987

[45] J. A. MacLachlan, J.-F. Ostiguy, *User's Guide to ESME2003*. Fermi National Accelerator Lab., Batavia, Illinois, 2003

[46] S. R. Koscielniak, *LONG1D User's Guide*. TRI-DN-97-12 v3.2, TRIUMF Vancouver, Canada, 2003

[47] A. Ando, K. Takayama, *$\bar{P}$ Bunch RF Rotation in the Debuncher Ring with Very Small η*. FERMILAB-TM-1073, Fermi National Accelerator Lab., Batavia, Illinois, 1981

[48] P. Lucas, J. A. MacLachlan, *Simulation of Space Charge Effects and Transition Crossing in the Fermilab Booster*. Part. Acc. Conf., Washington, D.C., 1987, pp. 1114-1116

[49] W. H. Press (ed.), Saul A. Teukolsky (ed.), W. T. Vetterling, B. P. Flannery, *Numerical Recipes in C++*. Camebridge University Press, Cambridge, U.K., 2nd ed., 2002, pp. 290-291

[50] P. M. Lapostolle, *Possible Emittance Increase through Filamentation due to Space Charge in Continous Beams*. IEEE Trans. Nucl. Sci., NS-18, 1971, pp. 1101-1104

[51] F. J. Sacherer, *RMS Envelope Equations with Space Charge*. IEEE Trans. Nucl. Sci., NS-18, 1971, pp. 1105-1107

[52] M. Weiss, *A Short Demonstration of Liouville's Theorem*. CERN 87-10, CERN Acc. School on Advanced Acc. Phys., Aarhus, Denmark, 1986, pp. 162-163

[53] S. van der Meer, *Stochastic Cooling of Betatron Oscillations in the ISR*. CERN/ISR-PO/72-31, CERN, Geneva, Switzerland, 1972

[54] S. van der Meer, *Stochastic Cooling and the Accumulation of Antiprotons*. In: Gösta Ekspong (ed.), *Nobel Lectures in Physics 1981-1990*. World Scientific, Singapore, Singapore, 1993, pp. 291-308

[55] G. I. Budker, *Status Report of Works on the Storage Rings at Novosibirsk*. Int. Symposium on Electron and Positron Storage Rings, Saclay, France, 1966, pp. II-1

[56] G. I. Budker, N. S. Dikansky, V. I. Kudelainen, I. N. Meshkov et al., *Experimental Studies of Electron Cooling*. Part. Acc., Vol. 7, 1976, pp. 197-211

[57] D. Neuffer, *Stability of Longitudinal Motion in Intense Ion Beams*. FERMILAB-FN-320, Fermi National Accelerator Lab., Batavia, Illinois, 1979

[58] A. Hofmann, F. Pedersen, *Bunches with Local Elliptic Energy Distributions*. IEEE Trans. Nucl. Sci., Vol. NS-26, 1979, pp. 3526-3528

[59] S. Hansen, H. G. Hereward, A. Hofmann, K. Hübner et al., *Effects of Space Charge and Reactive Wall Impedance on Bunched Beams*. IEEE Trans. Nucl. Sci., Vol. NS-22, 1975, pp. 1381-1384

[60] C. E. Nielsen, A. M. Sessler, *Longitudinal Space Charge Effects in Particle Accelerators*. Rev. Sci. Instr., Vol. 30, 1959, pp. 80-89

[61] V. K. Neil, A. N. Sessler, *Longitudinal Resistive Instabilities of Intense Coasting Beams in Particle Accelerators*. Rev. Sci. Instr., Vol. 36, 1965, pp. 429-436

[62] A. M. Sessler, V. G. Vaccaro, *Passive Compensation of Longitudinal Space Charge Effects in Circular Accelerators: The Helical Insert*. CERN 68-1, CERN, Geneva, Switzerland, 1968

[63] M. A. Plum, D. H. Fitzgerald, J. Langenbrunner, R. J. Macek et al., *Experimental Study of Passive Compensation of Space Charge at the Los Alamos National Laboratory Proton Storage Ring*. Phys. Rev. Special Topics - Acc. and Beams, Vol. 2, 1999, pp. 064201

[64] J.R. Maidment, E.A. Karantzoulis, *Longitudinal Space Charge via Multi Particle Simulation*. DESY HERA 88-09, Europ. Part. Acc. Conf., Rome, Italy, 1988, pp. 782-784

[65] R. Bossart, J. Bosser, L. Burnod, R. Coïsson et al., *Observation of Visible Synchrotron Radiation Emitted by a High-Energy Proton Beam at the Edge of a Magnetic Field*. Nucl. Instr. Meth., Vol. 164, 1979, pp. 375-380

[66] M. Sands, *The Physics of Electron Storage Rings*. SLAC-121, SLAC, Stanford, California, 1970, pp. 98-103

[67] C. G. Lilliequist, K. R. Symon, *Deviations from Adiabatic Behaviour during Capture of Particles into an R. F. Bucket*. MURA-491, Midwestern Universities Research Association, Madison, Wisconsin, 1959.

[68] R. Garoby, *RF Gymnastics in a Synchrotron*. In: A. W. Chao (ed.), M. Tigner (ed.), *Handbook of Accelerator Physics and Engineering*. World Scientific, Singapore, Singapore, 1998, pp. 287-292

[69] M. Bouthéon, J. Gareyte, *Adiabatic Trapping in the CERN PS*. Conf. High Energy Acc., Geneva, Switzerland, 1971, pp. 94-97

[70] H. Damerau, M. Emmerling, *Emittanzoptimierter Hochfrequenz-Einfang bei niedriger Strahlintensität*. SIS08012.HF, GSI Darmstadt, Germany, 2002

[71] D. G. Edwards, *Theoretical RF Trapping Behaviour for Various Time Functions of RF Voltage and Stable Phase Angle Without and With Space Charge Forces*. MPS/BR Note/73-17, CERN, Geneva, Switzerland, 1973

[72] I. Bozsik, I. Hofmann, A. Jahnke, R. W. Müller, *Numerical Investigation of Bunch-Merging in a Heavy-Ion-Synchrotron*. Proc. of Computing in Acc. Design and Operation, Berlin, 1983, pp. 128-133

[73] R. Garoby, *New RF Exercises Envisaged in the CERN-PS for the Antiprotrons Production Beam of the ACOL Machine*. IEEE Trans. Nucl. Sci., Vol. NS-32, 1985, pp. 2332-2334

[74] R. Garoby, *Bunch Merging and Splitting Techniques in the Injectors for High Energy Hadron Colliders*. CERN/PS 98-048(RF), Int. Conf. High Energy Acc., Dubna, Russia, 1998, pp. 172-174

[75] R. Garoby, *LHC Proton Beams in the PS: Status of Preparation and Capabilities*. CERN-AB-2003-008-ADM, LHC Performance Workshop, Chamonix XII, Chamonix, France, 2003, pp. 34-37

[76] R. Garoby, *Multiple Splitting in the PS: Results and Plans*. CERN-SL-2001-003 DI, LHC Workshop Chamonix, Chamonix XI, Chamonix, France 2001, pp. 32-36

[77] H. Damerau, *Vorschlag einer 20→1-Bunchmerging-Prozedur für die Vorbereitung des Strahls zur Bunchkompression im SIS100*. SIS25102.HF, GSI Darmstadt, Germany, 2002

[78] M. Benedikt, S. Hancock, J.-L. Vallet, *A Proof of Principle of Asymmteric Bunch Pair Merging*. AB-Note-2003-080 MD, CERN, Geneva, Switzerland, 2002

[79] C. Carli, *Creation of Hollow Bunches using a Double Harmonic RF System*. CERN/PS 2001-73 (AE), CERN Geneva, Switzerland, 2003

[80] C. Carli, M. Channel, *Creation of Hollow Bunches by Redistribution of Phase Space Surfaces*. CERN/PS 2002-19 (AE), Europ. Part. Acc. Conf., Vienna, Austria, 2000, pp. 233-235

[81] R. Garoby, *Proposal for a new Process Realizing Longitudinal Merging of Bunches in the CPS, while Conserving the Total Longitudinal Emittance of the Beam*. PS/RF/Note 83-15, CERN, Geneva, Switzerland, 1983

[82] R. Cappi, B. J. Evans, R. Garoby, *Status of the Anti-Proton Production Beam in the CERN PS*. Part. Acc., 1990, Vol. 26, pp. 217-222

[83] B. Autin, B. Bianchi, R. Billinge, D. Blechschmidt et al., *Design Study for a Proton-Antiproton Colliding Beam Facility*. CERN/PS/AA 78-3, CERN, Geneva, Switzerland, 1978, pp. 84-86

[84] G. Wiesenfeldt, *Untersuchungen zur longitudinalen Strahlanpassung beim Protonentransfer von PETRA nach HERA*. Diploma thesis, University of Hamburg, Germany, 1995

[85] E. J. N. Wilson (ed.), *Design Study of an Antiproton Collector for the Antiproton Accumulator (ACOL)*. CERN 83-10, CERN, Geneva, Switzerland, 1983, pp. 14-16

[86] P. J. Bryant, K. Johnsen, *The Principles of Circular Accelerators and Storage Rings*. Cambridge University Press, Cambridge, U.K., 1993, pp. 281-284

[87] K. M. Fung, M. Ball, C. M. Chu, B. Hamilton et al., *Bunch Length Compression Manipulations*. Phys. Rev. Special Topics - Acc. and Beams, Vol. 3, 2000, pp. 100101

[88] R. Garoby, *Une Procédure de Fabrication de Paquets Courts dans le PS*. PS/LR/Note 79-16, CERN, Geneva, Switzerland, 1979

[89] G. Franchetti, I. Hofmann, G. Rumolo, *Effect of Space Charge on Bunch Compression near Transition*. Phys. Rev. Special Topics - Acc. and Beams, Vol. 3, 2000, pp. 084201

[90] K. Y. Ng, *Space-Charge Effects on the Bunch Rotation in the Longitudinal Phase Space*. Part. Acc. Conf., Chicago, Illinois, 2001, pp. 2893-2895

[91] K. Y. Ng, *Space-Charge Effects on Bunch Compression*. FERMILAB-FN-702, Fermi National Accelerator Lab., Batavia, Illinois, 2001

[92] E. Shaposhnikova, *Time Scales for the Motion of Uncaptured Particles With RF Off and RF On in LHC*. LHC Project Note 281, CERN, Geneva, Switzerland, 2002

[93] D. Boussard, *RF for $p\bar{p}$ (Part II)*. CERN/SPS/84-2 ARF, CERN, Geneva, Switzerland, 1984

[94] M. Tigner, *Improved Method for Filling an Electron Storage Ring from a Synchrotron*. Part. Acc., Vol. 6, 1975, pp. 211-212

[95] J. E. Griffin, J. MacLachlan, A. G. Ruggiero, K. Takayama, *Time and Momentum Exchange for Production and Collection of Intense Antiproton Beams at Fermilab*. IEEE Trans. Nucl. Sci., Vol. NS-30, 1983, pp. 2630-2632

[96] J. E. Griffin, J. A. MacLachlan, G. N. Nicholls, Z. B. Qian, *Bunch Coalescing in the Main Ring to Form Intense Proton and Antiproton Bunches Without RF Counterphasing*. FERMILAB-TM-1280, Fermi National Accelerator Lab., Batavia, Illinois, 1984

[97] D. Wildman, P. Martin, K. Meisner, H. W. Miller, *Bunch Coalescing in the Fermilab Main Ring*. Part. Acc. Conf., Washington, D.C., 1987, pp. 1028-1030

[98] D. Boussard, J. Gareyte, P. Lefèvre, D. Möhl, *Une Procédure d'Accélération des Antiprotons via le PS*. PS/DL/Note 78-2, CERN, Geneva, Switzerland, 1978

[99] R. Garoby, *La Recombinaison Longitudinale dans le PS, Principe et Mise en Œvre Pratique*. CERN/PS/LR/Note 80-9, CERN, Geneva, Switzerland, 1980

[100] C. Ankenbrandt, *"Slip-Stacking": A New Method of Momentum-Stacking*. FERMILAB-FN-352, Fermi National Accelerator Lab., Batavia, Illinois, 1981

[101] D. Boussard, Y. Mizumachi, *Production of Beams with High Line-Density by Azimuthal Combination of Bunches in a Synchrotron*. CERN-SPS/ARF/79-11, IEEE Trans. Nucl. Sci., Vol. NS-26, 1979, pp. 3623-3625

[102] D. Boussard, Y. Mizumachi, *Numerical Computation of the Behaviour of Bunches in the Azimuthal Combination Processes*. SPS/ARF/YM/gs/Int. Note/79-12, CERN, Geneva, Switzerland, 1979

[103] K. Koba, J. Steimel, *Slip Stacking*. FERMILAB-Conf-02/205, 20th ICFA Advanced Beam Dynamics Workshop on High Intensity and High Brightness Hadron Beams, Fermi National Accelerator Lab., Batavia, Illinois, 2002, in: AIP Conf. Proc. 642, 2003, pp. 223-225

[104] K. Takayama, J. Kishiro, *Induction Synchrotron*. Nucl. Instr. Meth. A, Vol. 451, 2000, pp. 304-317

[105] U. Oeftiger, I. Hofmann, R. W. Müller, W. Pirkl, *Longitudinal Particle Dynamics in the HIDIF Driver Accelerator*. Nucl. Instr. Meth. A, Vol. 415, 1998, pp. 444-449

[106] G. W. Foster, C. M. Bhat, B. Chase, K. Seiya et al., *Beam Manipulation and Compression Using Broadband RF Systems in the Fermilab Main Injector and Recycler*. Europ. Part. Acc. Conf., Lucerne, Switzerland, 2004, pp. 1479-1481

[107] J. A. MacLachlan, *RF Stacking Without Emittance Dilution*. FERMILAB-Conf-00/117, American Physical Society April Meeting, Long Beach, California, 2000, in: Bull. Am. Phys. Soc., Vol. 45, 2000, p. 84

[108] W. Chou, J. Griffin, K. Y. Ng, D. Wildman et al., *Barrier RF Stacking at Fermilab*. Part. Acc. Conf., Portland, Orgegon, 2003, pp. 2922-2924

[109] C. M. Bhat, *A New Scheme for Momentum Mining of Beam Particles in a Storage Ring*. FERMILAB-FN-0746, Fermi National Accelerator Lab., Batavia, Illinois, 2004

[110] C. M. Bhat, *Longitudinal Momentum Mining in of Beam Particles in a Storage Ring*. FERMILAB-Pub-04/077-AD, Fermi National Accelerator Lab., Batavia, Illinois, 2004

[111] D. Broemmelsiek, M. Hu, S. Nagaitsev, *Stochastic Cooling in Barrier Buckets at the Fermilab Recycler*. Europ. Part. Acc. Conf., Lucerne, Switzerland, 2004, pp. 794-796

[112] J. Griffin, *Momentum Stacking in the Main Injector Using Longitudinal Barriers*. Fermi National Accelerator Lab., Batavia, Illinois, 2002, unpublished

[113] K. Y. Ng, *Continous Multiple Injection at the Main Injector*. Phys. Rev. Special Topics - Acc. and Beams, Vol. 5, 2002, pp. 061002

[114] K. Y. Ng, *Continous Multiple Injection at the Main Injector*. FERMILAB-FN-0715, Fermi National Accelerator Lab., Batavia, Illinois, 2002

[115] K. Y. Ng, *Doubling Main Injector Beam Intensity using RF Barriers*. FERMILAB-Conf-02/222, 20th ICFA Advanced Beam Dynamics Workshop on High Intensity and High Brightness Hadron Beams, Fermi National Accelerator Lab., Batavia, Illinois, 2002, in: AIP Conf. Proc. 642, 2003, pp. 226-228

[116] K. Y. Ng, *Double Intensity Injection for Antiproton Production*. FERMILAB-TM-2183, Fermi National Accelerator Lab., Batavia, Illinois, 2002

[117] see [15], p. 132

[118] J. Tückmantel, *The SPS/LHC Longitudinal Interface*. CERN-SL-99-007-DI, 9th LEP-SPS Performance Workshop, Chamonix IX, Chamonix, France, 1999, pp. 61-68

[119] O. Brüning, R. Cappi, R. Garoby, O. Gröbner et al., *LHC Luminosity and Energy Upgrade: A Feasibility Study*. LHC Project Report 626, CERN, Geneva, Switzerland, 2002

[120] F. Ruggiero, *LHC Accelerator R&D and Upgrade Scenarios*. LHC Project Report 666, Int. Symp. on LHC Physics and Detectors, Fermi National Accelerator Lab., Batavia, Illinois, 2003, in: Europ. Phys. Journal C - Particles and Fields, Vol. 34, 2004, pp. 433-442

[121] W. C. Middelkoop, A. Schoch, *Interaction Rate in Colliding Beam Systems*. AR/Int. SG/63-40, CERN, Geneva, Switzerland, 1963

[122] T. Suzuki, *General Formulae of Luminosity for Various Types of Colliding Beam Machines*. KEK-76-3, KEK, Tsukuba, Japan, 1976

[123] E. Keil, *Luminosity Optimisation for Storage Rings with Low-β Sections and Small Crossing Angles*. Nucl. Instr. Meth., Vol. 113, 1973, pp. 333-339

[124] L. Smith, *On the Calculation of Luminosity for Electron-Proton Colliding Beam*. PEP Note-20, Lawrence Berkeley Lab., Berkeley, California, 1972

[125] F. Ruggiero, G. Rumolo, F. Zimmermann, Y. Papaphilippou, *Beam Dynamics Studies for Uniform (Hollow) Bunches or Superbunches in the LHC: Beam-Beam Effects, Electron Cloud, Longitudinal Dynamics and Intrabeam Scattering*. LHC Project Report 627, Int. Workshop on Recent Progress in Induction Accelerators, Tsukuba, Ibaraki, Japan, 2002, pp. 131-147

[126] F. Ruggiero, F. Zimmermann, *Luminosity Optimization near the Beam-Beam Limit by Increasing Bunch Length or Crossing Angle*. Phys. Rev. Special Topics - Acc. and Beams, Vol. 5, 2002, pp. 061001

[127] see [119], p. 9

[128] E. Keil, *Beam-Beam Dynamics*. CERN 95-06, CERN Acc. School on Advanced Acc. Phys., Rhodes, Greece, 1993, pp. 539-555

[129] G. Guignard, *Review of the Investigation of the Beam-Beam Interactions at the ISR*. CERN ISR-BOM/79-28, Symposium on Nonlinear Orbit Dynamics and the Beam-Beam Interaction, Brookhaven Nat. Lab., Upton, New York, in: AIP Conf. Proc. 57, 1979, pp. 69-83

[130] L. R. Evans, J. Gareyte, *Beam-Beam Effects*. CERN 87-03, CERN Acc. School on Advanced Acc. Phys., Oxford, England, 1985, pp. 159-186

[131] K. Cornelis, L. Evans, A. Faugier, R. Schmidt, *Beam-Beam Effects and High Luminosity Operation in the SPS Proton Antiproton Collider*. CERN SPS/86-14 (MS), CERN, Geneva, Switzerland, 1986

[132] R. Schmidt, *Beam-Beam Observation in the SPS Proton Antiproton Collider*. Part. Acc., Vol. 50, 1995, pp. 47-60

[133] X. Zhang, T. Sen, V. Shiltsev, M. Xiao et al., *Experimental Studies of Beam-Beam Effects in the Tevatron*. Part. Acc. Conf., Portland, Orgegon, 2003, pp. 1757-1759

[134] T. Sen, B. Erdelyi, M. Xiao, V. Boocha, *Beam-beam effects at the Fermilab Tevatron: Theory*. Phys. Rev. Special Topics - Acc. and Beams, Vol. 27, 2004, pp. 041001

[135] W. Herr, *Tune Shifts and Spreads due to Short and Long Range Beam-Beam Interactions in the LHC*. CERN SL/90-06 (AP), LHC Note 119, CERN, Geneva, Switzerland, 1990

[136] F. Ruggiero, F. Zimmermann, G. Rumolo, Y. Papaphilippou, *Beam-Beam Interaction, Electron Cloud and Intrabeam Scattering for Proton Super-Bunches*. CERN-AB-2003-037 ABP, Part. Acc. Conf., Portland, Orgegon, 2003, pp. 123-125

[137] W. Herr, *Beam-Beam Effects in the LHC*. Part. Acc., Vol. 50, 1995, pp. 69-81

[138] K. Cornelis, W. Herr, M. Meddahi, *Proton Antiproton Collisions at a Finite Crossing Angle in the SPS*. Part. Acc. Conf., San Francisco, California, 1991, pp. 153-155

[139] K. Eggert, K. Honkavaara, A. Morsch, *Luminosity Considerations for the LHC*. CERN AT/94-04 (DI), LHC Note 263, CERN, Geneva, Switzerland, 1994

[140] H. Grote, W. Herr, *Nominal and Ultimate Luminosity Performance of the LHC*. LHC Project Note 275, CERN, Geneva, Switzerland, 2002

[141] A. Piwinski, *Abhängigkeit der Speicherring-Luminosität von der Taillenweite und vom Kreuzungswinkel*. DESY 67/7, DESY, Hamburg, Germany, 1967

[142] A. Piwinski, *Limitation of the Luminosity by Satellite Resonances*. DESY 77/18, DESY, Hamburg, Germany, 1977

[143] J. Strait, M. Lamm, P. Limon, M. V. Mokhov et al., *Towards a New LHC Interaction Region Design for a Luminosity Upgrade*. LHC Project Report 643, Part. Acc. Conf., Portland, Orgegon, 2003, pp. 42-44

[144] K. Takayama, *Super-bunch Hadron Colliders*. Int. Workshop on Recent Progress in Induction Accelerators, Tsukuba, Ibaraki, Japan, 2002, pp. 39-46

[145] R. Cappi, R. Garoby, S. Hancock, M. Martini et al., *The PS Complex as Part of the LHC Injector Chain*. CERN PS/91-07 (PA), CERN, Geneva, Switzerland, 1991

[146] M. Benedikt, A. Blas, J. Borburgh, R. Cappi et al., *The PS Complex as Proton Pre-Injector for the LHC - Design and Implementation Report*. CERN 2000-03, CERN, Geneva, Switzerland, 2000

[147] G. Arduini, *Beam Quality Preservation in the CERN PS-SPS Complex*. Europ. Part. Acc. Conf., Lucerne, Switzerland, 2004, pp. 78-82

[148] P. Collier (ed.), B. Goddard, R. Jung, K. H. Kissler, *The SPS as Injector for LHC, Conceptual Design*. CERN-SL-97-07 DI, CERN, Geneva, Switzerland, 1997

[149] E. Boltezar, H. Haseroth, W. Pirkl, G. Plass et al., *The New CERN* 50 *MeV Linac*. BNL-51134, Lin. Acc. Conf, Montauk, New York, 1979, pp. 66-77

[150] Study Group for CPS Improvements, *The Second Stage CPS Improvement Study* 800 *MeV Booster Synchrotron*. MPS/Int. DL/B 67-19, CERN, Geneva, Switzerland, 1967

[151] K. Schindl, *The PS Booster as Pre-Injector for LHC*. Part. Acc., Vol. 58, 1997, pp. 63-78

[152] J. M. Baillod, M. Corcelle, P. Gourcy, A. Krusche et al., *The Low Frequency Fundamental RF System for the LHC Beam Tests in the PSB*. PS/RF/Note 94-09, CERN, Geneva, Switzerland, 1994

[153] J. M. Baillod, M. Corcelle, P. Gourcy, A. Krusche et al., *The Second Harmonic RF System for the LHC Beam Tests in the PSB*. PS/RF/Note 94-10, CERN, Geneva, Switzerland, 1994

[154] A. Krusche, M. Paoluzzi, *The New Low Frequency Accelerating Systems for the CERN PS Booster*. CERN/PS 98-026 (RF), Europ. Part. Acc. Conf., Stockholm, Sweden, 1998, pp. 1782-1783

[155] A. Hofmann, S. Myers, *Calculation of the RF and Beam Parameters for the Double RF System*. LEP Note 158, CERN, Geneva, Switzerland, 1979

[156] A. Hofmann, S. Myers, *Beam Dynamics in a Double RF System*. CERN ISR-TH-RF/80-26, Conf. High Energy Acc., CERN, Geneva, 1980, pp. 610-614

[157] E. Regenstreif, *Le Synchrotron à Protons du CERN (1ère Partie)*. CERN 58-6 a, CERN, Geneva, Switzerland, 1958

[158] E. Regenstreif, *Le Synchrotron à Protons du CERN (2ème Partie)*. CERN 59-26, CERN, Geneva, Switzerland, 1959

[159] E. Regenstreif, *Le Synchrotron à Protons du CERN (3ème Partie)*. CERN 61-9, CERN, Geneva, Switzerland, 1961

[160] R. Cappi, *The PS in the LHC Injector Chain*. Part. Acc., Vol. 58, 1997, pp. 79-89

[161] R. Garoby, J. Jamsek, P. Konrad, G. Lobeau et al., *RF System for High Beam Intensity Acceleration in the CERN PS*. CERN/PS 89-28(HF), Part. Acc. Conf., Chicago, Illinois, 1989, pp. 135-137

[162] D. Grier, *The PS 10 MHz Cavity and Power Amplifier*. PS/RF Note 2002-073, CERN, Geneva, Switzerland, 2002

[163] R. Garoby, S. Hancock, J.-L. Vallet, *Demonstration of Bunch Triple Splitting in the CERN PS*. Europ. Part. Acc. Conf., Vienna, Austria, 2000, pp. 304-306

[164] R. Garoby, *Requirements to the PS RF System for Filling the LHC with 25 ns Spacing between Bunches*. PS/RF/Note 93-04, CERN, Geneva, Switzerland, 1993

[165] R. Garoby, *A Non-Adiabatic Procedure in the PS to Supply the Nominal Proton Bunches for LHC into 200 MHz RF Buckets in SPS*. PS/RF/Note 93-17, CERN, Geneva, Switzerland, 1993

[166] M. Benedikt, R. Cappi, M. Chanel, R. Garoby et al., *Performance of the LHC Pre-Injectors*. CERN-PS-2001-011 (DR), High Energy Acc. Conf., Tsukuba, Japan, 2001, pp. MO-09

[167] CERN, *The 300 GeV Programme*. CERN/1050, CERN, Geneva, Switzerland, 1971

[168] T. Bohl, T. Linnecar, E. Shaposhnikova, *Study of Different Operating Modes of the 4th RF Harmonic Landau Damping System in the CERN SPS*. CERN-SL-98-026 RF, Europ. Part. Acc. Conf., Stockholm, Sweden, 1998, pp. 978-980

[169] P. Baudrenghien, T. Bohl, T. Linnecar, E. Shaposhnikova et al., *Nominal Longitudinal Parameters for the LHC Beam in the CERN SPS*. Part. Acc. Conf., Portland, Orgegon, 2003, pp. 3050-3052

[170] D. Boussard, T. Linnecar, *The LHC Superconducting RF System*. LHC Project Report 316, Cryogening Engineering and Int. Cryogenic Materials Conf., Montreal, Canada, 1999, in: Advances in Cryogenic Engineering, Vol. 45 A, pp. 835-844

[171] R. Bailey, P. Collier, *Standard Filling Schemes for Various LHC Operation Modes (Revised)*. LHC-Project Note 323_Revised, CERN, Geneva, Switzerland, 2003

[172] P. Collier, *Baseline Proton Filling Schemes*. CERN-AB-2004-014 ADM, LHC Performance Workshop, Chamonix XIII, Chamonix, France, 2004, pp. 30-33

[173] see [14], p. 46

[174] J. M. Jowett, *Collision Schedules for the LHC*. Beam Physics Note 21, CERN, Geneva, Switzerland, 1999

[175] M. Benedikt, K. Cornelis, R. Garoby, E. Métral et al., *Report of the High Intensity Protons Working Group*. CERN-AB-2004-022 OP/RF, CERN, Geneva, Switzerland, 2004

[176] H. Damerau, R. Garoby, *Reference Scheme for Barrier Bucket RF Gymnastics in the LHC*. Internal note, in preparation

[177] J. Tückmantel, *Simulation of LHC with a Realistic RF System*. CERN-SL-2001-003 DI, LHC Workshop Chamonix, Chamonix XI, Chamonix, France 2001, pp. 306-311

[178] T. Bohl, *A Superconducting RF Cavity for Bunch Compression of the High Intensity SPS Proton Beam at Transfer to LHC*. Europ. Part. Acc. Conf., Sitges, Spain, 1996, pp. 2094-2096

[179] S. Wolfram, *Mathematica: A System for Doing Mathematics by Computer*. Addison-Wesley, Redwood City, California, 1988

[180] R. Garoby, D. Grier, E. Jensen, A. Mitra et al., *The PS 40 MHz Bunching Cavity*. Part. Acc. Conf., Vancouver, Canada, 1997, pp. 2953-2955

[181] E. Jensen, R. Hohbach, A. K. Mitra, R. L. Poirier, *Higher Order Mode Damping of the CERN PS 40 MHz Cavity*. Europ. Part. Acc. Conf., Sitges, Spain, 1996, pp. 2068-2070

[182] D. Grier, E. Jensen, R. Losito, A. K. Mitra, *The PS 80 MHz Cavities*. Part. Acc. Conf., Stockholm, Sweden, 1998, pp. 1773-1775

[183] The CERN Study Group on New Accelerators, *Report on The Design Study of Intersecting Storage Rings (ISR) for the CERN Proton Synchrotron*. CERN/542, AR/Int. SG/64-9, CERN Geneva, Switzerland, 1964

[184] K. Johnsen, *28 GeV Intersecting Proton Storage Rings at CERN*. Conf. High Energy Acc., Yerevan-Tsahkadzor, Russia, 1969, Vol. II, pp. 131-144

[185] K. Johnsen, *The CERN Intersecting Storage Rings*. Conf. High Energy Acc., Geneva, Switzerland, 1971, pp. 79-84

[186] A. Hofmann, *Single-Beam Collective Phenomena - Longitudinal*. CERN 77-13, 1st Course of the Int. School on Part. Acc. Phys., Erice, Italy, 1976, pp. 139-174

[187] A. Sessler, V. Vaccaro, *Longitudinal Instabilities of Azimuthally Uniform Beams in Circular Vacuum Chambers with Walls of Arbitrary Electrical Properties*. CERN 67-2, CERN, Geneva, 1967

[188] E. Keil, W. Schnell, *Concering Longitudinal Stability in the ISR*. CERN-ISR-TH-RF/69-48, CERN, Geneva, Switzerland, 1969

[189] K. Hübner, V. G. Vaccaro, *Dispersion Relations and Stability of Coasting Particle Beams*. CERN-ISR-TH/70-44, CERN, Geneva, Switzerland, 1970

[190] A. G. Ruggiero, V. G. Vaccaro, *Solution of the Displersion Relation for Longitudinal Stability of an Intense Coasting Beam in a Circular Accelerator (Application to the ISR)*. ISR-TH/68-33, CERN, Geneva, Switzerland, 1968

[191] B. Zotter, *Longitudinal Stability Diagrams for Some Particular Distribution Functions*. CERN/ISR-GS/76-11, CERN, Geneva, Switzerland, 1976

[192] W. Schnell, *Stacking and Acceleration*. BNL 20550, Proc. 1975 Isabelle Summer Study, Brookhaven Nat. Lab., Upton, New York, 1975, pp. 126-132

[193] D. Boussard, *Observation of Microwave Longitudinal Instablilities in the CPS*. CERN LABII/RF/Int./75-2, CERN, Geneva, Switzerland, 1975

[194] K. Hübner, B. Zotter, *Microwave Instability Criteria for Bunches Proton Beams*. CERN/ISR-TH/78-3, CERN, Geneva, Switzerland, 1978

[195] J. M. Wang, C. Pellegrini, *On the Condition for a Single Bunch High Frequency Fast Blow-up*. Conf. High Energy Acc., Geneva, Switzerland, 1980, pp. 554-561

[196] E. Shaposhnikova, *Signatures of the Microwave Instability*. CERN-SL-99-008 HRF, Joint US-CERN-Japan-Russia Particle Accelerators School on Beam Measurement, Montreux, Switzerland, 1998, pp. 351-377

[197] see [15], p. 101

[198] L. D. Landau, *On the Vibrations of the Electronic Plasma*. J. Phys. U.S.S.R, Vol. 10, 1946, pp. 25-34, in: D. Ter Haar (ed.), *Collected Papers of L. D. Landau*. Pergamon Press, Oxford, 1965, pp. 445-460

[199] H. G. Hereward, *The Elementary Theory of Landau Damping*. CERN 65-32, CERN, Geneva, Switzerland, 1965

[200] A. Hofmann, *Landau Damping*. CERN 89-01, CERN Acc. School on Acc. Phys., Berlin, Germany, 1989, pp. 40-56

[201] A. Hofmann, *Landau Damping*. CERN 95-06, CERN Acc. School on Advanced Acc. Phys., Rhodes, Greece, 1993, pp. 275-305

[202] F. J. Sacherer, *A Longitudinal Stability Criterion for Bunched Beams*. CERN/MPS/Int. BR/73-3, IEEE Trans. Nucl. Sci., Vol. NS-20, 1973, pp. 825-829

[203] Y. Baconnier, D. Boussard, J. Gareyte, *Some Preliminary Results on Coherent Longitudinal Instabilities in the CPS*. CERN/MPS/SR 70-6, CERN, Geneva, Switzerland, 1970

[204] F. Sacherer, *Methods for Computing Bunched-Beam Instabilities*. CERN/SI-BR/72-5, CERN, Geneva, Switzerland, 1972

[205] F. Sacherer, *Bunch Lengthening and Microwave Instability*. CERN/PS/BR/77-5, IEEE Trans. Nucl. Sci., Vol. NS-24, 1977, pp. 1393-1395

[206] F. Sacherer, *Bunch Lengthening and Microwave Instability (Part 2)*. CERN/PS/BR 77-06, CERN, Geneva, Switzerland, 1977

[207] K. Y. Ng, *Introduction to Collective Instabilities - Longitudinal and Transverse*. FERMILAB-TM-2053, Overseas Chinese Phys. Association Accelerator School, Hsinchu, Taiwan, 1998

[208] J. L. Laclare, *Bunched-Beam Instabilities, Memorial Talk for F. J. Sacherer*. Int. Conf. High Energy Acc., Geneva, Switzerland, 1980, pp. 526-539

[209] F. Ruggiero, *Single-Beam Collective Effects in the LHC*. CERN SL/95-06 (AP), LHC Note 313, Part. Acc., Vol. 50, 1995, pp. 83-104

[210] E. Shaposhnikova, personal communication, 2003, see also: V. I. Balbekov, S. V. Ivanov, *Longitudinal Beam Instabilities in Proton Synchrotrons*. Conf. High Energy Acc., Novosibirsk, Russia, 1983, pp. 124-129

[211] D. Boussard, D. Brandt, L. Vos, *Is a Longitudinal Feedback Required for LHC?* LHC Project Note 205, CERN, Geneva, Switzerland, 1999

[212] E. Shaposhnikova, *Longitudinal Beam Parameters during Acceleration in the LHC*. LHC Project Note 242, CERN, Geneva, Switzerland, 2000

[213] E. Shaposhnikova, *Longitudinal Phenomena during the LHC Cycle*. CERN-SL-2001-003 DI, LHC Workshop Chamonix, Chamonix XI, Chamonix, France 2001, pp. 312-316

[214] D. Angal-Kalinin, L. Vos, *Coupled Bunch Instabilities in the LHC*. LHC Project Report 585, Europ. Part. Acc. Conf., Paris, France, 2002, pp. 290-292

[215] D. Angal-Kalinin, D. Brandt, L. Vos, *Intermediate Review of Single Bunch Collective Effects in the LHC*. LHC Project Report 587, Europ. Part. Acc. Conf., Paris, France, 2002, pp. 305-307

[216] D. Angal-Kalinin, *Review of Coupled Bunch Instabilities in the LHC*. LHC Project Report 595, CERN, Geneva, Switzerland, 2002

[217] L. Bottura, P. Burla, R. Wolf, *LHC Main Dipoles Proposed Baseline Current Ramping*. LHC Project Report 172, CERN, Geneva, Switzerland, 1998

[218] D. Boussard, E. Chiaveri, H. P. Kindermann, T. Linnecar et al., *Design Condiderations for the LHC 200 MHz RF System*. LHC Project Report 368, CERN, Geneva, Switzerland, 2000

[219] R. Losito, E. Chiaveri, R. Hanni, T. Linnecar et al., *Industrial Production of Eight Normal-Conducting 200 MHz ACN Cavities for the LHC*. Europ. Part. Acc. Conf., Lucerne, Switzerland, 2004, pp. 956-958

[220] T. Linnecar, *RF Capture and Synchronization*. CERN-AB-2003-008-ADM, LHC Performance Workshop, Chamonix XII, Chamonix, France, 2003, pp. 234-237

[221] P. B. Wilson, *Theory and Design of Superconducting Electron Linear Accelerators*. In: Septier, A. L. (ed.), P. M. Lapostolle, *Linear Accelerators*. North-Holland Publ. Co., Amsterdam, Netherlands, 1970, pp. 1107-1140

[222] J. Tückmantel, *Operating an LHC RF Station on a Sideband or with Amplitude-Modulation*. AB-Note-2004-045 RF, CERN, Geneva, Switzerland, 2004

[223] J. Tückmantel, *Consequences of an RF Power Trip in LHC*. AB-Note-2004-008, CERN, Geneva, Switzerland, 2004

[224] H. P. Kindermann, M. Stirbet, *The Variable Power Coupler for the LHC Superconducting Cavity*. CERN-SL-99-074 HRF, 9th Worshop on RF Superconductivity, Santa Fe, New Mexico, 1999, pp. 566-569

[225] P. B. Wilson, *Transient Beam Loading in Electron-Positron Storage Rings*. CERN-ISR-TH/78-23 (Rev.), CERN, Geneva, Switzerland, 1978

[226] J. Tückmantel, *Realistic RF System and Beam Simulation in Real Time for a Synchrotron*. CERN-SL-2001-007 HRF, High Energy Acc. Conf., Tsukuba, Japan, 2001, pp. P2hc07

[227] J. Tückmantel, *The LHC Beam with Suppressed RF Transients*. AB-Note-2004-22 RF, CERN, Geneva, Switzerland, 2004

[228] V. Rödel, L. Verolino, *Geometry of a 400 MHz Feedback Cavity for the LHC*. SL/RFS/Note 91-10, CERN, Geneva, Switzerland, 1991

[229] W. Höfle, *RF-Power Requirements for the LHC Bunch to Bunch Longitudinal Feedback-System*. SL/Note 94-60, CERN, Geneva, Switzerland, 1994

[230] J. B. Adams, J. V. Allaby, F. Amman, F. Bonaudi et al., *A Design of the European 300 GeV Research Facilities*. CERN/MC/60, CERN, Geneva, Switzerland, Vol. 1/2, 1970

[231] G. Arduini, P. Baudrenghien, T. Bohl, P. Collier et al., *Status of the LHC Proton Beam in the CERN SPS*. Europ. Part. Acc. Conf., Paris, France, 2002, pp. 206-208

[232] G. Arduini, P. Baudrenghien, T. Bohl, P. Collier et al., *The LHC Proton Beam in the CERN SPS: An Update*. Part. Acc. Conf., Portland, Oregon, 2003, pp. 1718-1720

[233] T. Bohl, T. Linnecar, E. Shaposhnikova, *Barrier buckets in the CERN SPS*. CERN-SL-2000-020 HRF, Europ. Part. Acc. Conf., Vienna, Austria, 2000, pp. 1220-1222

[234] T. Bohl, T. Linnecar, E. Shaposhnikova, *Thick barrier buckets using the SPS travelling wave structures*. CERN SL-Note-2000-032 HRF, CERN Geneva, Switzerland, 2000

[235] T. Bohl, T. Linnecar, E. Shaposhnikova, *Impedance Reduction in the CERN SPS as Seen from Longitudinal Beam Measurements*. CERN-SL-2002-023 (HRF), Part. Acc. Conf., Vienna, Austria, 2000, pp. 1446-1448

[236] T. Bohl, H. Damerau, R. Garoby, T. Linnecar et al., *MD on Barrier Buckets in the SPS*. AB-Note-2003-096 (MD), CERN, Geneva, Switzerland, 2003

[237] T. Bohl, H. Damerau, R. Garoby, T. Linnecar et al., *Barrier Buckets and Transient Beam Loading in the SPS*. CERN-AB-2004-008, CERN Geneva, Switzerland, 2004

[238] G. Dôme, *The SPS Acceleration System Travelling Wave Drift-Tube Structure for the CERN SPS*. CERN-SPS/ARF/77-11, Proton Linear Accelerator Conference, Chalk River, Ontario, Canada, 1976, pp. 138-147

[239] D. Boussard, *Beam loading*. CERN 95-06, CERN Acc. School on Advanced Acc. Physics, Rhodes, Greece, 1993, pp. 415-436

[240] P. Baudrenghien, G. Lambert, *Reducing the impedance of the Travelling Wave Cavities: Feed-forward and one turn delay feed-back*. CERN-SL-2000-007-DI, 10th Workshop on LEP-SPS Performance, Chamonix X, Chamonix, France 2000, pp. 94-101

[241] National Accelerator Laboratory, *Design Report*. National Accelerator Laboratory, Batavia, Illinois, 1968, pp. 9-26 to 9-30

[242] R. Garoby, *Longitudinal Limitations in the PS Complex for the Generation of the LHC Proton Beam*. Part. Acc., Vol. 58, 1997, pp. 121-136

[243] Gesellschaft für Schwerionenforschung mbH, *An International Accelerator Facility for Beams of Ions and Antiprotons*. GSI Conceptual Design Report, 2001, pp. 535-537

[244] P.Spiller, K. Blasche, U. Blell, O. Boine-Frankenheim et al., *SIS100/300 Conceptual Design Studies*. GSI Report 2004-1, GSI, Darmstadt, 2004, pp. 249-250

[245] see [243], pp. 528-531

[246] J. M. Baillod, L. Magnani, G. Nassibian, F. Pedersen et al., *A Second Harmonic (6-16 MHz) RF System with Feedback-Reduced Gap Impedance for Accelerating Flat-Topped Bunches in the CERN PS Booster*. IEEE Trans. Nucl. Sci., Vol. NS-30, 1983, pp. 3499-3501

[247] A. Blas, S. Hancock, M. Lindroos, *Hollow Bunch Distributions at High Intensities in the PS Booster*. Europ. Part. Acc. Conf., Vienna, Austria, 2000, pp. 1528-1530

[248] S. Y. Lee, *Accelerator Physics*. World Scientific, Singapore, 1999, p. 234-235, p. 241

[249] F. Kuypers, *Klassische Mechanik*. Wiley-VCH, Weinheim, 5. ed., 1997, pp. 331-332

[250] H.L. Hagedoorn, J. I. M. Botman, W. J. G. M. Kleeven, *Hamiltonian Theory is a Tool for Accelerator Physics*. CERN 92-01, CERN Acc. School on Advanced Acc. Phys., Noordwijkerhout, Netherlands, 1991, pp. 1-50

[251] B. Zotter, *BBI - A Program to Compute Bunches Beam Instabilities in High Energy Particle Accelerators and Storage Rings*. CERN LEP/TH 89-74, CERN, Geneva, Switzerland, 1989

[252] G. Besnier, *Contribution à la Théorie de la Stabilité des Oscillations Longitudinales d'un Faisceau Accéléré en régime de charge d'espace*. Thèse, Université de Rennes 1, 1978, p. 12

[253] Klaus Wille, *Physik der Teilchenbeschleuniger und Synchrotronstrahlungsquellen*. Teubner Verlag, Stuttgart, Germany, 1996, 2nd ed., pp. 130-132

[254] cf. [86], pp. 100-101

[255] P. Schmüser, *Basic Course on Accelerator Optics*. CERN 94-01, CERN Acc. School on General Acc. Phys., Jykväskylä, Finland, 1992, pp. 17-88

[256] E. Wilson, *Transverse Beam Dynamics*. CERN 94-01, CERN Acc. School on General Acc. Phys., Jykväskylä, Finland, 1992, pp. 131-158

[257] see [248], p. 91-92

[258] L. J. Laslett, *On the Limitations Imposed by Transverse Space-Charge Effects in Circular Particle Accelerators*. BNL 7534, Proc. 1963 Summer Study on Storage Rings, Accelerators and Experimentation at Super-High Energies, 1963, BNL, Upton, New York, pp. 324-367

[259] K. Schindl, *Space Charge*. CERN-PS-99-012-DI, Joint US-CERN-Japan-Russia Particle Accelerators School on Beam Measurement, Montreux, Switzerland, 1998, pp. 127-151

[260] M. Reiser, *Theory and Design of Charged Particle Beams*. Wiley-Interscience, New York, New York, 1994, pp. 260-273

Acknowledgements

This is dedicated to all those who have contributed to make this work possible:

First of all, I would like to acknowledge Prof. Dr. Thomas Weiland (Darmstadt University of Technology) for his advice and support during the studies for this thesis.

I am thankful to Prof. Dr. Klaus Wille (University of Dortmund) for accepting to serve as second examiner.

It is a great pleasure to thank Roland Garoby who supervised the thesis project at CERN. His continuous interest, dedicated ideas and straightforward guidance based on his deep insight into the physics of particle accelerators were invaluable to keep the studies right on track.

I am grateful to Dr. Elena Shaposhnikova for many stimulating discussions on longitudinal beam instabilities, and to Drs. Thomas Bohl, Steven Hancock, Joachim Tückmantel who illuminated innumerous details of the RF systems at CERN and their interaction with the particle beam. I am also indebted to Dr. Frank Zimmermann for helpful explanations of luminosity and beam-beam effects.

I am thankful to Drs. Andreas Jankowiak (University of Mainz), Juris Kaugerts (GSI), Boris Keil (PSI) and Gerald Schreiber (GSI) for the proof-reading of this report.

Finally, I would like to acknowledge GSI, Darmstadt for supporting the studies at CERN.

Curriculum Vitae

Personal data

Name:	Heiko Damerau
Born on:	21 December 1974 in Lünen

Education and professional experience

2003 – 2004	Delegated as associate to the radio frequency group at CERN, Geneva, Switzerland
2001	Participant of the CERN Accelerator School, *Intermediate Accelerator Physics Course*, Sevilla, Spain
2001 – 2005	Graduate studies of accelerator physics Darmstadt University of Technology, Darmstadt, Germany and scientific employee in the radio frequency group at GSI, Darmstadt, Germany
2001	Diploma thesis, *Entwicklung eines subharmonischen Bunchkompressionssystems für das Booster-Synchrotron BoDo bei DELTA*, University of Dortmund, Dortmund, Germany
2000	Participant of the CERN Accelerator School, *RF Engineering*, Seeheim, Germany
1999 – 2000	Diploma student in the accelerator group of the Dortmund Electron Test Facility (DELTA), University of Dortmund, Dortmund, Germany
1995 – 2001	Studies of physics University of Dortmund, Dortmund, Germany